INFORMATION TO USERS

This manuscript has been reproduced from the microfilm master. UMI films the text directly from the original or copy submitted. Thus, some thesis and dissertation copies are in typewriter face, while others may be from any type of computer printer.

The quality of this reproduction is dependent upon the quality of the copy submitted. Broken or indistinct print, colored or poor quality illustrations and photographs, print bleedthrough, substandard margins, and improper alignment can adversely affect reproduction.

In the unlikely event that the author did not send UMI a complete manuscript and there are missing pages, these will be noted. Also, if unauthorized copyright material had to be removed, a note will indicate the deletion.

Oversize materials (e.g., maps, drawings, charts) are reproduced by sectioning the original, beginning at the upper left-hand corner and continuing from left to right in equal sections with small overlaps.

Photographs included in the original manuscript have been reproduced xerographically in this copy. Higher quality 6" x 9" black and white photographic prints are available for any photographs or illustrations appearing in this copy for an additional charge. Contact UMI directly to order.

Bell & Howell Information and Learning
300 North Zeeb Road, Ann Arbor, MI 48106-1346 USA

UMI®
800-521-0600

HAWKING RADIATION PHOTOSPHERE

AROUND

MICROSCOPIC BLACK HOLES

Michael Mostoslavsky

Physics Department
McGill University
Montréal

March 1998

A thesis submitted to the Faculty of Graduate Studies and Research
in partial fulfillment of the requirements
of the degree of Master of Science.

Abstract

The Boltzmann equation for the diffusion of Hawking radiation from microscopic black holes is solved using the test particle method. Formation of a dense cloud of interacting particles analogous to the photosphere of the Sun is confirmed. We find that at least two kinds of photospheres may form: a quark-gluon plasma for black holes of mass $M_{BH} \lesssim 5 \times 10^{14}$ g and an electron-positron-photon plasma for $M_{BH} \lesssim 2 \times 10^{12}$ g. The QCD photosphere extends from the black hole horizon for a distance of 0.2–4.0 fm for 10^9 g $\lesssim M_{BH} \lesssim 5 \times 10^{14}$ g, at which point quarks and gluons with average energy of order Λ_{QCD} hadronize. The QED photosphere starts at a distance of approximately 700 black hole radii and dissipates at about 400 fm, where the average energy of the emitted electrons, positrons and photons is inversely proportional to the black hole temperature. Possible consequences of these photospheres are discussed.

Résumé

Le spectre de radiation de Hawking des trous noirs microscopiques est calculé par résolution numérique de l'équation de Boltzmann en utilisant la méthode des particules tests. Nous confirmons la formation autour du trou noir d'un nuage dense de particules en intéraction, analogue à la photosphère solaire. Deux types de photosphères peuvent finalement apparaitre: Un plasma de quarks et gluons pour des trous noirs de masse $M_{BH} \lesssim 5 \times 10^{14}$ g et un plasma d'électrons, positrons et photons pour les trous noirs de masse $M_{BH} \lesssim 2 \times 10^{12}$ g . La première photosphère, obtenue dans le cadre de QCD, s'étend depuis l'horizon du trou noir sur une distance de 0.2–4 fm pour 10^9 g $\lesssim M_{BH} \lesssim 5 \times 10^{14}$ g. Au delà, il y a hadronisation des quarks et gluons dont l'energie est de l'ordre de Λ_{QCD}. La photosphère QED nait à une distance d'environ 700 fois le rayon du trou noir et se dissipe autour de 400 fm où lénergie des électrons, positrons et photons est inversement proportionnelle à la température du trou noir. D'éventuelles conséquences de l'existence de telles photosphères sont discutées.

Aknowledgments

First, and foremost, I would like to thank my supervisor, Prof. Jim Cline, whose financial support, competent guidance and most essential collaboration made this work possible from the beginning to the end. Equally, if not more, important to me were his tolerance and respect towards my countless personal and professional faults. I am sorry that my appreciation was seldom expressed. Also, I'm grateful to him and to the Department of Physics for giving me the opportunity to live in a wonderful city of Montréal, which brought a lot of joy and comfort into my life.

I want to thank Geraldine Servant who got this project started and contributed ideas, energy and work to all of its parts. In fact, the development of the method and the computer code was done in close collaboration with her. She made this work fun and became a personal friend. Thank you, Jim, for introducing us.

My special thanks go to Ioulia Kvasnikova and Karina Chobanian who gave me all the support I needed to write this thesis. They had changed me and my life and I'll always be grateful for that. I also thank Ioulia for countless valuable professional suggestions and last minute proofreading of the thesis.

Words can not express all my gratitude to my parents, Yuri and Veronika Mostoslavsky, whose support was felt and appreciated in spite of thousands of kilometers between us.

I met so many friendly people at the Physics Department that it would be unfair to mention but a few. Dr. Mohammad Zebarjad, however, stands out. Always helpful professionally, for the three years we shared an office, he has been the source of kind humor and a willing party to the most interesting and inspiring conversations. I'll miss you Mohammad. Neither can I forget to mention Denis Michaud, Martin Kamela, Guy Michaud and, of course, Andrew Hare. A lot of thanks are due to our graduate secretary Paula Domingues.

Contents

Chapter 1

Introduction

One of the beautifully exotic consequences of the Einstein's general relativity is the prediction of the existence of black holes. Whenever matter of mass M is concentrated in a region whose circumference in any direction is smaller than $2\pi(2GM/c^2)$ it gets trapped inside the Schwarzchild horizon

$$r_h = \frac{2G}{c^2}M \tag{1.1}$$

and becomes a black hole. The constant, $2G/c^2 \sim 10^{-30}$ m/g, is so small that for the mass of our Sun the radius of the horizon is $r_{h_\odot} \simeq 3$ km.

It had been long believed that nothing can escape from inside the black hole horizon and hence we can get no direct evidence of black hole existence. However, in 1974 Stephen Hawking [1] mathematically showed that in a startling interplay between quantum mechanics and general relativity black holes must radiate energy as an almost perfect black body with temperature

$$T_{BH} = \frac{\hbar c^3}{8\pi k_B G M}. \tag{1.2}$$

The rate of emission from an uncharged, non-rotating black hole is

$$\frac{dN}{dEdt} = \frac{\sigma_s(E)E^2}{2\pi}\frac{1}{\exp(E/T_{BH}) - (-1)^{2s}}, \tag{1.3}$$

for a particle of spin s with energy in the range $(E, E+dE)$, where $\sigma_s(E)$ is absorption cross section for the same particle by the black hole.

In the last equation we have used natural units, as we will throughout the thesis, so that $\hbar = 1$, $c = 1$ and $k_B = 1$. The following relations between black hole

parameters are given in these units [2]. The temperature in GeV of a black hole of mass M(in g) is

$$T_{BH} = 0.1 \text{ GeV} \left(\frac{10^{15} \text{ g}}{M}\right); \tag{1.4}$$

the Schwarzchild horizon of a black hole is

$$r_h = \frac{1}{4\pi T_{BH}} = 1.57 \text{ fm} \left(\frac{\text{GeV}}{T_{BH}}\right); \tag{1.5}$$

these units are relevant for the microscopic black holes to be studied in this thesis. The luminosity is

$$L = 10^{26} \frac{\text{MeV}}{\text{s}} \left(\frac{10^{15} \text{ g}}{M}\right)^2 \tag{1.6}$$

Finally, since a black hole is constantly radiating energy, it will evaporate completely after a lifetime of

$$t = 10^{10} \text{ yr} \left(\frac{M}{10^{15} \text{ g}}\right)^3 \tag{1.7}$$

It is easy to see from these formulas that Hawking radiation is extremely weak and hence undetectable for very massive black holes. For example, for a black hole of solar-mass size ($M_\odot \simeq 10^{30}$ g, $r_{h_\odot} \simeq 3$ km) — not particularly massive on the cosmic scale, — the luminosity is mere 10^{-4} eV/s. So if we want to detect particles escaping from black holes they must have much smaller masses than $M_\odot$. However, in the present day universe, black holes may be formed only in gravitational collapse of stars heavier than $\sim 3M_\odot$ and so a recently formed black hole is not a good source of detectable Hawking radiation [2]. But the hope should not be abandoned, for it has been suggested that in the early universe other black hole formation mechanisms were available, as, for example, the collapse of overdense regions in a universe with significant density fluctuations [3, 4, 5]. Black holes formed in the early universe are called primordial and can have mass as low as the Planck mass (2.2×10^{-5} g) [2].

The luminosity of microscopic primordial black holes is very high [see Eq. (1.6)], so that Hawking radiation is the crucial factor in their evolution. In fact, according to Eq. (1.7), all primordial black holes of mass smaller than $\sim 10^{15}$ must have evaporated entirely before any human ever came to think about them. Those that were initially slightly more massive, though, would now be in the final stage of their existence, which is rather violent: in its last second a black hole of initial mass 10^{16}g would radiate about 10^{23}J of energy, so that for a brief moment it would be comparable in luminosity to a small star [6]. Knowing the spectrum of such energy burst would

allow us to look for them in the sky. Also, the radiation of primordial black holes that are extinct by now might have contributed to the extragalactic γ-ray background. To address these issues we need to know the detailed spectrum of black hole emission.

A thorough investigation was done after Hawking radiation was first suggested [7, 8, 9]. For example, Page in [10] gave numerical calculations of the emission rates for massless particles. He concluded that 81% of total power emitted by a massive ($M \gg 10^{17}$g) black hole is in neutrinos, 17% in photons and 2% in gravitons; for lighter, but still-evaporating black holes ($5 \times 10^{14}\text{g} \ll M \ll 10^{17}\text{g}$), 45% of the power is in electrons and positrons, 45% in neutrinos, 9% in photons and 1% in gravitons.

For massive particles, the early approach was to assume that any particle species is emitted according to Eq. (1.3) once the black hole temperature exceeds the relevant rest mass [8, 11]. As suggested by MacGibbon and Weber in [12], this might not be true for particles with composite structure. For black hole temperatures of order Λ_{QCD} and higher, relativistic quark and gluon jets are emitted which subsequently fragment into the stable photons, leptons and hadrons. In [12] the final emission spectra were obtained by convolving the Hawking radiation formula with a Monte Carlo QCD jet code for jet fragmentation. MacGibbon and Carr in [13] described how the final stable particles are affected by interactions with the rest of the universe and gave detailed results of primordial black hole emission contribution to the extragalactic γ-ray and electron, positron and antiproton backgrounds. They also concluded that the direct explosive emission from an individual hole is not likely to be detected above the cosmic-ray backgrounds.

Radiation from very high temperature black holes was estimated by Oliensis and Hill in [14]. The contribution of such black holes to ultrahigh-energy cosmic rays was found to be insignificant. It was also pointed out that the high energy radiation emitted by a real black hole is expected to be non-thermal.

From this review we see that the spectrum of primordial black holes may be quite different from the thermal distributions, for example, if quark-gluon fragmentation is considered. In this thesis, we explore another possibility of changing the spectrum of the initially emitted Hawking radiation: interactions between the emitted particles while they emerge from the vicinity of the black hole.

Chapter 2

Do Black Holes Have Photospheres?

In January 1997 Andrew Heckler suggested that the observed black hole radiation spectrum may be quite different from that at the horizon if the emitted particles start *interacting with one another* as they propagate away and do so strongly enough to form a photosphere [15]. This possibility had been previously argued against. In the first section we examine the arguments that had led to this conclusion and Heckler's arguments to the contrary. A brief account of the photosphere as emerges from his analysis is given in the second one.

2.1 Interactions

Authors prior to Heckler did consider the possibility of interactions. MacGibbon and Carr in [13] extensively investigated interactions of the particles emitted by primordial black holes with *other particles in the universe.* For example, photons from primordial black holes can be scattered through (1) ionization and photoelectric absorption, dominant for photon energy $E_\gamma \lesssim 14$ keV; (2) Compton scattering off electrons: 14 keV $\lesssim E_\gamma \lesssim$ 65 MeV; (3) pair production off nuclei: 65 MeV $\lesssim E_\gamma \lesssim$ 2 TeV; (4) pair production off the 3K background photons: $E_\gamma \gtrsim 2$ TeV. However, neither these nor any of the interactions of other emitted particles with the rest of the universe were concluded to significantly change the spectrum of primordial black holes.

Oliensis and Hill [14] also considered interactions. Even though their paper deals with ultra high energy radiation, i.e. very hot black holes $T_{BH} \gg 100$GeV, they argue that particles emitted from any black hole would be able to interact with one another if the time between subsequent emissions is small compared to $t = r/c$, where r is the range of the interaction and $c = 1$ is the speed of light (all relevant particles being relativistic). It is expected that $t \simeq 1/E$, where $E \sim T_{BH}$. It is also estimated that the time between emissions is $dt = 200/8\pi E \sim 8/E$. Therefore, "since $dt \gg 1/E$, a black hole at a given temperature radiates particles infrequently compared to their

average energy and these particles will tend not to interact before fragmenting". Another argument for the same conclusion is the finite size of the hole, which might be thought to prevent particles emitted from opposite sides from interacting with each other.

The arguments and conclusions of both papers are true, with one exception. They fail for a particular kind of interaction: bremsstrahlung (and the closely related process of photon-electron pair production, see diagram on p. 18), which turns out to be important at least for three reasons.

1. It is not $2 \rightarrow 2$ body scattering (as for example, Compton scattering), but $2 \rightarrow 3$, i.e. a new particle takes some energy every time an interaction has taken place. This can reduce the average particle energy dramatically.

2. At relativistic energies the energy-averaged bremsstrahlung cross section is only logarithmically dependent on the energy, and so the decrease in particle energy described above will not affect by much the probability of interactions.

3. The range of interaction for bremsstrahlung is not $1/E$ as was estimated in [14], but $1/m_e$. Black hole temperatures of interest are $T_{BH} \gtrsim \Lambda_{QCD} \simeq 200$ MeV, so the time between emissions is $dt \simeq 8/E \ll 1/m_e$, which is the condition mentioned earlier for the interactions to become important.

So the conclusion that made the present work possible is that interactions of emitted particles with one another may become very important if bremsstrahlung and photon-electron (quark-gluon for QCD) pair production are taken into account. The arguments leading to this conclusion are somewhat elaborated in the next section and discussed in great detail in Chapter 4.

2.2 Photosphere Hypothesis

It is thus claimed that for a certain black hole temperature there will be enough particles to produce a dense interacting cloud which will certainly change the emission spectrum of an individual black hole. This cloud was called a photosphere in analogy with that of the Sun, where particles emitted from the core scatter and lose energy on their way out. In this section I will briefly review how Heckler in [15] analytically justified the existence and analyzed the properties of a photosphere around a microscopic black hole.

We begin by discussing the simple case of QED only. A black hole of temperature T_{BH} greater than the electron mass emits electrons, positrons and photons which will all be treated as "particles". Suppose that at the horizon their energy spectrum and density are thermal (up to grey-body factors) with temperature T_{BH}. Going away from the horizon they scatter via bremsstrahlung ($e^{\pm} + e^{\pm} \rightarrow e^{\pm}e^{\pm}\gamma$) and photon-electron pair production ($e^{\pm} + \gamma \rightarrow e^{\pm}e^{+}e^{-}$) which are both $2 \rightarrow 3$ body interactions

with cross section which depends only logarithmically on the energy. Total energy-averaged cross section for both interactions is approximately

$$\sigma \approx 8\alpha r_e^2 \ln \frac{2E}{m_e}, \tag{2.1}$$

where E is the energy in the center-of-mass frame and $r_e = \alpha/m_e$ is the classical electron radius.

Let $\mathcal{N}(r)$ be the number of scatterings an average particle has undergone by the time it reaches radius r. If λ is the mean free path, then

$$\mathcal{N}(r) = \int_{r_{BH}}^{r} \frac{dr}{\lambda(r)}. \tag{2.2}$$

If $\mathcal{N}$ becomes greater than 1 for $r = \infty$ we can say that some kind of photosphere has formed: on average every particle has interacted before escaping. Calculating $\mathcal{N}(\infty)$ naively, neglecting plasma effects and density enhancement due to particle production, yields:

$$\mathcal{N}_{brem} \approx \frac{\alpha^3}{2\pi^4} \frac{T_{BH}}{m_{0_e}} \ln \frac{2T_{BH}}{m_{0_e}}, \tag{2.3}$$

where m_{0_e} is vacuum electron mass. The *critical temperature*, — the black hole temperature for which $\mathcal{N}(\infty) \simeq 1$,— is found to be $T_c \sim 20$ TeV.

To improve this estimate we have to take account of the fact that bremsstrahlung processes occur not in vacuum but in a background plasma of almost radially propagating particles. The thermal mass could be used for this purpose, so that the electron mass becomes

$$m_e^2 = m_{0_e}^2 + m_{pm}^2(n, T, p), \tag{2.4}$$

where a simple estimate for the plasma mass m_{pm} of an electron in a plasma with density $n(r)$ is

$$m_{pm}^2 \approx \frac{4\pi\alpha n(r)}{\overline{E}}. \tag{2.5}$$

The average energy $\overline{E}$ of a particle emitted from a black hole is $\sim 5T_{BH}$ and since it decreases with each scattering, through conservation of energy it is estimated to be $\overline{E} \approx 5T_{BH}/(3/2)^{\mathcal{N}}$ [15].

Both mean free path and plasma mass depend on density $n(r)$, which increases each time a new particle is created (but, of course, decreases with radial expansion). Taking both effects into account, the density of particles can be estimated as

$$n(r) = \left(\frac{3}{2}\right)^{\mathcal{N}(r)} \frac{r_{BH}^2}{r^2}\, n_h, \tag{2.6}$$

where n_h is the density at the horizon. The improved formula for $\mathcal{N}$ is

$$\mathcal{N}(r) \approx 8\alpha^3 \int_{r_{BH}}^{r} dr \frac{n(r)}{m_e^2(r)} \ln \frac{2T_{BH}}{m_e(r)}, \tag{2.7}$$

where the plasma mass of the electron depends on the distance through density.

To find the critical black hole temperature ($\mathcal{N}_{T_c}(\infty) = 1$), Eq. (2.7) was solved both numerically and analytically and it was found that

$$T_c \simeq 45 \text{ GeV}. \tag{2.8}$$

The numerical result for this and two other black hole temperatures is illustrated by Fig. 2.1 reproduced from [15]. We shall see in Chapter 5 that using our test particle model of the photosphere we obtained very similar results (cf. Fig. 5.1). Ref. [15] proceeds by modeling the photosphere formed for $T_{BH} > T_c$ as a thick shell of plasma and uses a fluid description to find the inner and outer radii of this shell. His results are:

$$r_0 \simeq \frac{4\pi}{\alpha^4 T_{BH}} \quad \text{and} \quad r_{edge} \simeq \frac{1}{\alpha^2 m_{0_e}} \left(\frac{T_{BH}}{T_c}\right)^{1/2}. \tag{2.9}$$

An observationally relevant quantity is the average particle energy at the edge of the photosphere:

$$\overline{E}_{edge} \simeq m_{0_e} \left(\frac{T_{BH}}{T_c}\right)^{1/2}. \tag{2.10}$$

We summarize these results for several black hole temperatures in the Table 2.2. Describing briefly Heckler's picture of the QED photosphere: for temperatures lower than 45 GeV, emitted particles free-stream away from the black hole and the observed spectrum is given by the Hawking formula; for temperatures greater than critical the particles begin to scatter significantly to form a partially-thermalized photosphere at a distance r_0 from the black hole. From there they make their way through plasma losing significant fraction of their energy in bremsstrahlung and electron-photon pair production. The edge of the plasma is at r_{edge}, where the average particle energy is reduced to the order of $m_{0_e} \ll T_c$. At this point electron and positron annihilate and the photons free stream away to infinity.

Ref. [15] suggests that to see more accurately what is happening in this plasma shell one would have to solve the Boltzmann equation, which is the subject of this

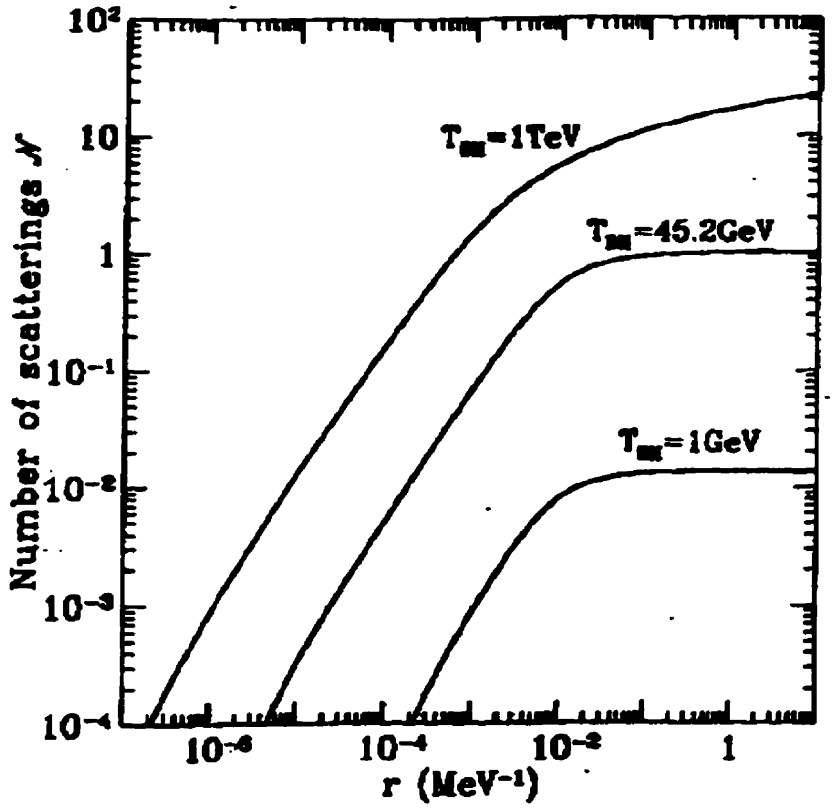

Figure 2.1: Numerical results of Ref. [15] for $\mathcal{N}(r)$ – the number of scatterings an average particle undergoes as it propagates to a distance r from the black hole horizon.

T_{BH}	r_0	r_{edge}	$\overline{E}_{edge}$
45 GeV	8×10^7 GeV^{-1}	9×10^7 GeV^{-1}	$m_{0_e} \simeq 5 \times 10^{-4}$ GeV
300 GeV	1.5×10^7 GeV^{-1}	1×10^8 GeV^{-1}	1.3×10^{-3} GeV
1000 GeV	4.5×10^6 GeV^{-1}	1.7×10^8 GeV^{-1}	2.4×10^{-3} GeV

Table 2.1: Photosphere parameters according to ref. [15] for several black hole temperatures.

thesis. As we will see, although his estimate for the critical temperature is very close to our value and the photosphere hypothesis seems to be correct, the photosphere parameters found in our model are very different from those given in Table 2.2, indicating that the fluid description is not valid.

Chapter 3

Test Particle Model

3.1 Boltzmann Equation

As was noted in the previous chapter, we would like to have a more quantitative picture of particle diffusion outside the Schwarzchild horizon, which would in particular confirm or refute the photosphere formation hypothesis. That picture could be provided by a solution to the Boltzmann equation:

$$(\frac{\partial}{\partial t} + \frac{\mathbf{p}}{E} \cdot \nabla) f(\mathbf{r}, \mathbf{p}, t) = C[f(\mathbf{r}, \mathbf{p}, t)], \tag{3.1}$$

where $f(\mathbf{r}, \mathbf{p}, t)$ is the particle distribution function, depending in general on particle position and momentum, and also on time; $C(f)$ is the collision term: a multidimensional phase space integral over distribution functions, weighted by the probability of the interactions between the particles.

To simplify the equation we can make certain assumptions about the black holes, namely:

A. We will consider only spherical, non-rotating black holes. Hence the distribution function for emitted radiation will be spherically symmetric:

$$\frac{\partial}{\partial \theta} f = \frac{\partial}{\partial \phi} f = \frac{\partial}{\partial p_\phi} f = 0. \tag{3.2}$$

B. Mass (temperature) of the black hole does not change significantly in the time interval needed for a particle originating at the horizon to reach the edge of the photosphere or, in other words, to become a virtually free particle. [1] This implies the time independence of the distribution function:

[1] For a typical black hole (M=10^{11}g, T=1000 GeV) this time interval is $\tau(\sim 10^{-21}) \ll t(\sim 10^5$ sec), black hole lifetime. We estimate that only for black holes of mass $\lesssim 10^7$g the lifetime will become comparable to the particle diffusion time in the photosphere.

$$\frac{\partial}{\partial t} f = 0. \tag{3.3}$$

The Boltzmann equation then reduces to

$$\frac{\partial}{\partial r} f(r, p_r, p_t) = \frac{1}{v_r} C(f(r, p_r, p_t)), \tag{3.4}$$

where $v_r = E/p_r$ is the particle's radial velocity.

Even in this form, though, it involves phase space integration in the collision term, has three independent variables and a partial derivative on the left-hand side which altogether make it a formidable task to solve the equation by direct numerical evolution of the distribution function. However, there has been suggested a way to circumvent this problem.

3.2 Test Particle Method

The test particle method of solving the Boltzmann equation was first used in the problem of heavy ion collisions [16]. The phase space distribution function of nucleons was represented by a set of point-like test particles. This set was then evolved using Hamilton's equations for free propagation between the collisions, and the two-body differential scattering cross section for the collision probability. It was argued that with a sufficiently large number of test particles this method provides a valid solution to the Boltzmann equation. But having more test particles than there are nucleons would artificially increase the probability of collisions if the naive interaction cross section was used in the collision term. Therefore an appropriate factor was used to reduce this probability.

There are two major differences between the heavy nucleus and the black hole radiation problems. The first one,— spatial homogeneity in the former and explicit spatial dependence (on r) in the latter, — actually turns to our advantage if we remember that we assumed the radiation to be in steady state [Eq. (3.3)]. If we compare the Boltzmann equation for $f = f(\mathbf{p}, t)$ (heavy nuclei):

$$\frac{\partial}{\partial t} f(\mathbf{p}, t) = C(f(\mathbf{p}, t)) \tag{3.5}$$

with the one we want to solve [Eq. (3.4)], we see that there is no reason why the method for solving the one would not work for the other, provided we consider radial diffusion instead of time evolution.

The second difference is that, for reasons to become apparent later, our cross section, and hence collision probability, will never in any way depend on the number

of test particles, but rather on the density of real radiation, which may be calculated independently of the model. Therefore, there is no need to "scale" cross section and any statistically reasonable number of test particles may be used.

3.3 Test Particles for Hawking Radiation

Even though the number of test particles will depend only on statistical considerations, their characteristics, i.e. mass, spin, interaction properties will be defined by the part of black hole radiation to be modeled in each particular case. For example, to establish existence of QED photosphere we will ignore all the particles emitted for a particular black hole temperature except electrons, positrons and photons. Then approximately two thirds of our test particles will be identified as electrons or positrons and one third as photons, and electromagnetic interactions will be used. For the QCD photosphere, another cage of the Hawking zoo is going to be looked at. To model quark and gluon diffusion, test particles will assume their respective properties and the appropriate strong interaction coupling constant will be used in formulas.

I would like, however, to start with a demonstration of how the method works in the case when it is not the nature of the test particles which is relevant but their classical propagation trajectory.

3.4 Free Evolution

It is important to realize that test particles are perfectly classical particles following well defined trajectories. In absence of interactions between the particles themselves or with external fields, they will move in straight lines. As we can see from Eq. (3.4) relevant phase space coordinates of a particle are p_r and p_t and we would like to know how those change (if at all) with our evolution coordinate r.

Let us look at a free particle starting at the horizon with momentum $\mathbf{p} = (p^r, p^t)$ (we are not interested in p^ϕ and can confine the problem to $(\mathbf{r}, \mathbf{p})$ plane). At radius $r > r_h$, momentum will remain the same, but its coordinates will change.

From Fig. 3.1 we see that

$$p^t = p \sin\alpha \qquad \text{and} \qquad \sin\theta = \frac{p_h^t}{p},$$

To write new momentum coordinates in terms of those at the horizon we use some geometry:

$$\frac{\sin\alpha}{r_h} = \frac{\sin\beta}{r}; \quad \sin\beta = \sin\theta; \quad \sin\alpha = \frac{r_h}{r}\sin\theta.$$

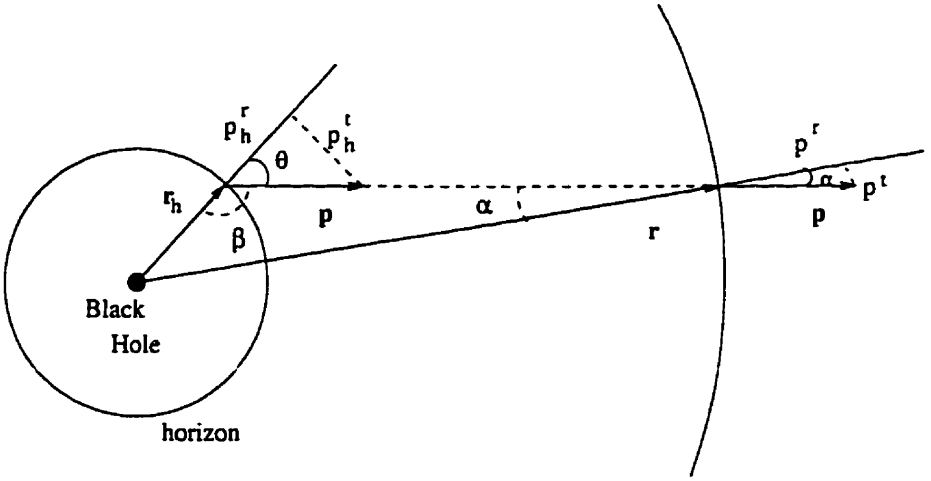

Figure 3.1: Momentum in free radial evolution

And finally we get:

$$p^t = \frac{r_h}{r} p_h^t \qquad \text{and} \qquad p^r = \sqrt{p^2 - p^{t2}}. \tag{3.6}$$

Note that these formulas are valid for any two r_h and r such that $r > r_h$ and we are going to use them when propagating test particles in radius between collisions.

We see that the transverse component dies out as $1/r$ and as a free particle is going away from the horizon its momentum becomes increasingly radial.

To solve the Boltzmann equation for radiation streaming free from a black hole we start at the horizon with a set of N particles. We propagate each of them to a new radius by changing their momentum coordinates according to the above formulas. With the new coordinates we can generate distribution functions which will be the solution to the free Boltzmann equation at the new radius.

3.5 Evolving interacting particles

The picture will be somewhat more complicated when the particles are allowed to interact. Even though we neglect external fields (black hole is not charged and its gravitational field is negligible in the region of interest), we do want to take scatterings into account and that changes the way the test particle method is implemented.

We start again at the Schwartzchild horizon with a set of statistically significant number of particles. To be specific, let us consider the case of the QED photosphere, where all black hole radiation is neglected except for electrons, positrons and photons. The number ratio of fermions to bosons was calculated to be 2:1 which means that two thirds of test particles at the horizon will assume electron properties and the

rest, those of the photon. We will refer to these test particles as "test-electrons" and "test-photons".

As we are modeling Hawking radiation, test-electron and test-photon energy distributions must obey Eq. (1.3) with $s = 1/2$ and $s = 1$ respectively at the horizon. To find the energy of each test particle we use a standard Monte Carlo technique described by MacGibbon and Weber in [12]. If Q is the particle energy and T is black hole temperature (fixed), a value for $X = Q/T$ is first randomly chosen between 0 and X_{max}, the maximum value of Q/T in the program ($10T$ in our case). An ensemble of such X values will be distributed according to

$$H(X) = \frac{\Gamma_s(X)X^2}{\exp(X) - (-1)^{2s}}, \tag{3.7}$$

if we require that $H(X) \geq H_{max}R$ where R is a random number between 0 and 1 and $H_{max} \geq$ the maximum of $H(X)$ for all X. To calculate the Γ_s factor we use averaged value for absorption cross section [12]:

$$\Gamma_s = \begin{cases} \frac{56.7}{27\pi} & \text{for fermions} \\ \\ \frac{20.4}{27\pi} & \text{for bosons.} \end{cases} \tag{3.8}$$

The next step after distributing the energies of the test particles is to assign momenta to all of them. To model isotropic radiation at the horizon we let our test particles start with momenta pointing in arbitrary directions uniformly distributed over outward-pointing solid angle of 2π steradians (Fig. 3.2). Since we already know the energy of each particle E we can just choose the radial component of the momentum $p^r = R\sqrt{E^2 - m^2}$ (where R is again a random number between 0 and 1), and then calculate the transverse component $p^t = \sqrt{E^2 - m^2 - p^{r2}}$. Note that $p^r \geq 0$ (particles are radiated, not absorbed) and $p^t \geq 0$ (by definition, see Fig. 3.2). This procedure is equivalent to choosing directions according to the measure $d(\cos\theta)$, where θ is defined by $\tan\theta = p^t/p^r$.

At this point we are ready to propagate the test particles away from the horizon. In the heavy ion problem, where time is the propagation parameter, an average time between the collisions is used as the propagation step. It is natural to use the mean free path, or some fraction thereof, as the increment in radius for our model. The propagation procedure goes as follows: in the beginning all the test particles are randomly paired. Then for each pair, the bremsstrahlung cross section σ, the relative velocity of the particles in the pair v_{rel} and the radial velocity ($1/v_r$ factor) are calculated. Mean free path is

$$\lambda = \left[n(r)\left\langle\frac{\sigma}{v_r}v_{rel}\right\rangle\right]^{-1}, \tag{3.9}$$

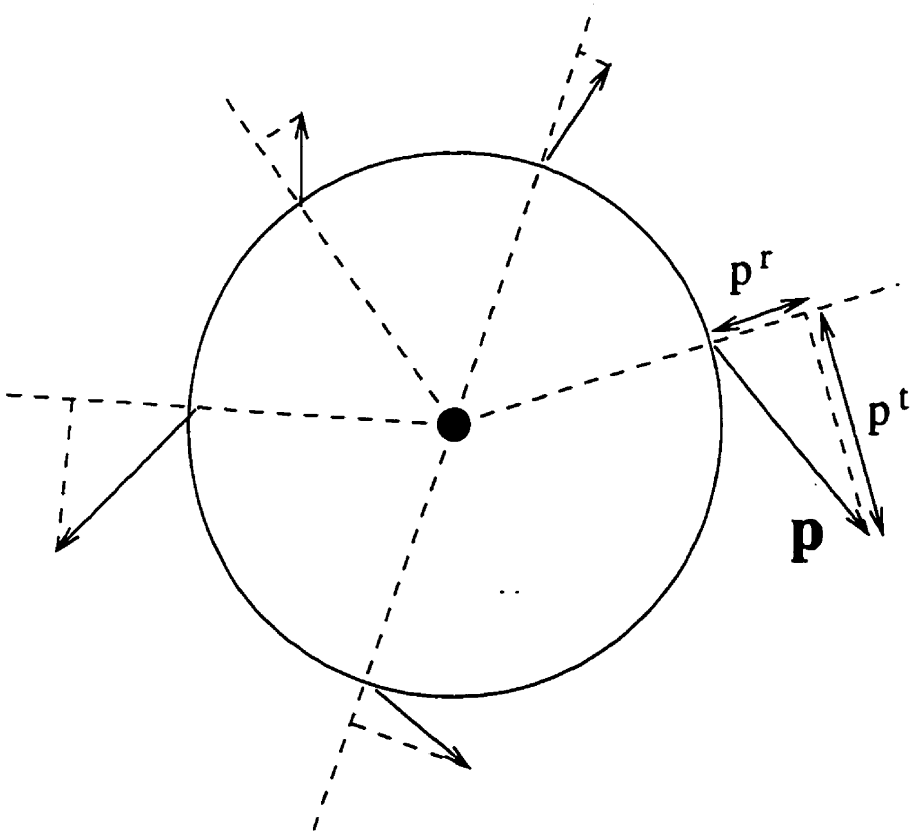

Figure 3.2: Test particle momenta at the horizon

where average is taken over all pairs. Details of these calculations are presented in Chapter 4. The particle density $n(r)$ is calculated analytically and therefore does not depend on the number of the test particles. To find $n(r)$ we first compute what it would be in the absence of particle production:

$$n_0(r) = n_h \frac{r_h^2}{r^2}, \tag{3.10}$$

where the subscript 0 means that this density is before particle creation process is taken into account. The radius of the horizon is $r_h = 1/(4\pi T_{BH})$ and the density at the horizon is

$$n_h = 2 \int \frac{d^3p}{(2\pi)^3} f(p), \tag{3.11}$$

where $f(p)$ is the Hawking distribution. Remembering that since the particles are being emitted outward, θ should only be integrated to $\pi/2$, we obtain:

$$n_h = \begin{cases} \frac{3}{\pi^2}\Gamma_f\,\zeta(3)\,T_{BH}^3 & \text{for fermions} \\ \\ \frac{2}{\pi^2}\Gamma_b\,\zeta(3)\,T_{BH}^3 & \text{for bosons,} \end{cases} \tag{3.12}$$

where $\zeta(3) = 1.20206$ (Rieman zeta function) and Γ_s is given in Eq. (3.8).

To account for particle creation we use the test particles to find the fraction of new fermions and bosons created at each step. Let $N_{f[b]}(r)$ be the number of test-electrons [test-photons] at radius r. We will define $R_{f[b]}(r)$ as:

$$R_{f[b]}(r) = \frac{N_{f[b]}(r)}{N_{f[b]}(r_h)}. \tag{3.13}$$

Finally, using (3.10) through (3.13) we find

$$n(r) = \frac{\zeta(3)}{\pi^2(4\pi)^2}\frac{T_{BH}}{r^2}\begin{cases} 3\Gamma_f\,R_f(r) & \text{for fermions} \\ \\ 2\Gamma_b\,R_b(r) & \text{for bosons.} \end{cases} \tag{3.14}$$

Once we have calculated the mean free path, we can propagate all the particles to the next step. For several reasons we decided to make this step a small fraction of λ. First, λ itself, which depends on r, increases significantly over propagation distance $\Delta r = \lambda$. Secondly, at each successive step we start by allowing all the test particles collide in pairs, whereas in reality, different pairs would interact at different points between r and $r + \lambda$.

If Δr is the step in radius we use and $f = \lambda/\Delta r$, then only N/f test particles should be allowed to collide at each step in radius. This factor f should be large enough so that $\lambda(r)$ does not increase too much before it is recalculated at the next step; on the other hand it should be small enough so that at least one pair interacts during the step. Comparing the results for different values of f, we found that for the QED photosphere they usually stabilized at $f \geq 50$, when the initial number of test particles was large enough to allow using f up to 100.

Kinematically, bremsstrahlung and pair production are modeled by an inelastic scattering of two test-electrons (one test-electron and one test-photon for pair production) in which a new test-photon (test electron pair instead of test photon) is created. Details of how it is done are discussed in Chapter 4. $N/2f$ pairs are sorted out at each step as those that have the highest probability to interact and their collisions are subsequently simulated. Then all the test particles are propagated to the next radius at $r + \Delta r$. Between colliding and reaching the new radius, test particle energies do not change but the coordinates of their momenta do, according to Eq. (3.6).

Let us summarize the algorithm for evolving the set of interacting test particles:

1. Particles are put randomly in pairs and the mean free path is calculated using Eq. (3.9).

2. All test particles are propagated as free to the new radius $r' = r + \lambda/f$ using (3.6).

3. Pairs are sorted by interaction probability.

4. $N/2f$ most probably interacting pairs are sent to the subroutine where bremsstrahlung or pair production (whichever is relevant for the specific pair) is modeled.

5. Back to step 1.

We start this procedure at the black hole horizon where the radiation is emitted and end it when mean free path starts to diverge so that only a negligible number of interactions would follow (see p. 31 for a more precise definition of the photosphere edge). For the QCD photosphere, however, long before this criterion is satisfied, the average particle energy drops below Λ_{QCD}, at which point hadronization occurs and quark-gluon photosphere ceases to exist (see chapter 6).

Now, that we have discussed the test particle method, we can turn to the physics of interactions which create the photosphere.

Chapter 4

Scatterings in detail

In this chapter we will discuss: why bremsstrahlung and electron-photon pair production are the dominant processes for photosphere production (Section 1); why the effective electron mass is much larger at the beginning of the photosphere than at the end (Section 2); how the bremsstrahlung cross section and mean free path are calculated (Section 3 and 4); and, finally, why all the particles in the photosphere scatter as though they were colliding head-on, and how these collisions are simulated for test particles (Section 5 and 6).

4.1 Interactions considered and neglected

In the test particle simulation of black hole radiation diffusion, one must decide which interactions to include in the collision term in the Boltzmann equation (3.4). Consider, for example, the case of QED, where the particles of interest are electrons, positrons and photons. Their dominant interactions are [17]:

1) Coulomb

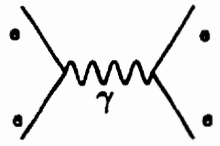

$$\sigma_{coul} \sim r_e^2 \frac{1}{\gamma^2}$$

2) Compton

$$\sigma_{com} \sim r_e^2 \frac{m_e}{\omega}$$

3) Bremsstrahlung and Pair Production

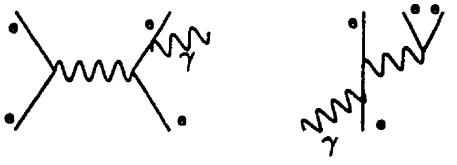

$$\sigma_{brem} \approx 8\alpha r_e^2 \ln \frac{2\omega}{m_e}$$

4) Electron-Positron Annihilation

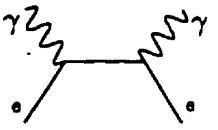

$$\sigma_{ann} \sim \frac{r_e^2}{\gamma},$$

where $r_e = \alpha/m_e$ is the classical electron radius, ω is the energy in the center of mass system, and β is the velocity of this system ($\gamma = (1-\beta^2)^{-1}$).

Let us start with annihilation. We argue that as long as photon energy is larger than the electron mass, the electron-positron annihilation will be in equilibrium with its inverse process, photon-photon pair production. In particular, emitted and created electrons and positrons will in the end annihilate only if the average photon energy falls below m_e before the photosphere dissipates for other reasons, which we find does not happen until the black hole is as hot as 10^8 GeV.

For production of the photosphere the most important reactions are those which can significantly change the particle energy spectrum. Bremsstrahlung (and pair production) is dominant in this sense, because every reaction produces a new particle which in turn reduces the average particle energy and shifts the spectrum towards lower energies. The cross sections for these processes depend only logarithmically on energy, and so are not much affected by this degradation in energy.

Because Compton scattering can neither change average energy nor increase the thermal mass, we ignore it for the time being, realizing though that a more accurate model would have to include these interactions.

As for Coulomb scattering, according to Haug [18], it can be considered as a correction factor to bremsstrahlung cross section, which can be found by calculating the ratio of probabilities of finding the two initial and final electrons, respectively, at the same position. This factor is approximately unity for higher energies.

So, in our simulation the only interactions we take into account will be bremsstrahlung and pair production, and as we will see those are sufficient to produce a photosphere.

4.2 Thermal Mass

In bremsstrahlung cross section and other formulas involving electron mass, the so called "thermal" (or effective) mass is used, related to the vacuum mass m_{0_e} by

$$m_e = \sqrt{m_{0_e}^2 + m_{pm}^2(n, T, p)}. \tag{4.1}$$

As was noted in Chapter 2, this is a way of including the effect of high density plasma on the interactions. Plasma mass m_{pm} is a function of density, temperature and momentum. It needs to be calculated for the kind of plasma that is created around a microscopic black hole: a nonthermal, largely radially-moving collection of relativistic particles. However, it is possible to justify the following estimate, which was derived in the case of thermal equilibrium [19]:

$$m_{pm}^2 = 4\pi\alpha \int d^3p \left(\frac{1}{2} \frac{f_f(p)}{p} + \frac{f_b(p)}{p} \right), \tag{4.2}$$

where $f_{f(b)}(p)$ is the distribution function for fermions (bosons). For a collection of test particles the integral may be approximated by taking the average of $1/p$ over all test-electrons and test-photons:

$$m_{pm}^2 \simeq 4\pi\alpha \left(\frac{1}{2} n_e \left\langle \frac{1}{p_e} \right\rangle + n_\gamma \left\langle \frac{1}{p_\gamma} \right\rangle \right). \tag{4.3}$$

Several aspects of the implementation of thermal mass in the test particle model are noteworthy. First, in Eq. (4.3) n_e and n_γ are real electron and photon densities calculated analytically [see Eq. (3.14)], whereas p_e and p_γ are kinetic energies of the test-particles. Secondly, we recalculate electron thermal mass [using Eq. (4.1)] at each step in radius. If its momentum was held fixed, this would change its total energy $E = \sqrt{m_e^2 + p_e^2}$, which we certainly want to be conserved. Hence, we assume that thermal mass correction is done at the expense of particle kinetic energy in such a way as to keep its total energy E constant.

We can estimate thermal mass of an electron in the QED photosphere using $n(r) = T_{BH}(3/2)^{\mathcal{N}(r)}/(\pi^2(4\pi)^2 r^2)$ for the densities of both photons and electrons, and $3T_{BH}/(3/2)^{\mathcal{N}(r)}$ for average particle energy at radius r. Here, $\mathcal{N}(r)$ is the number of scatterings an average particle undergoes between the horizon and radius r. Since in each scattering one new particle is produced, $(3/2)^{\mathcal{N}(r)}$ is the factor by which the total number of particles has increased. In the test-particle model, since the total number of particles $N(r)$ is known at each step, this increase is calculated directly as $N(r)/N(r_h)$. Then,

$$m_e \simeq \sqrt{m_{0_e}^2 + \frac{\alpha}{\pi(4\pi)^2} \frac{1}{r^2} \left(\frac{N(r)}{N(r_h)} \right)^2}. \tag{4.4}$$

The behavior of thermal mass is shown in Fig. 4.1. The graphs are of effective mass vs. radius for two typical photospheres: QED photosphere of a 1000 GeV black

hole and QCD photosphere of a 10 GeV black hole. We see that in the QED plasma the factor of $1/r^2$ is dominant over any growth in density as the radius increases, which causes the thermal mass to decrease monotonically. On the other hand, in the QCD plasma, the particle production factor $N(r)/N(r_h)$ is more influential (due to dependence of the average particle energy on the coupling constant, in particular) and just before the hadronization begins to occur ($\langle E \rangle \sim \Lambda_{QCD}$) thermal mass may again become very high. The perturbative formulas leading to this should not be believed however.

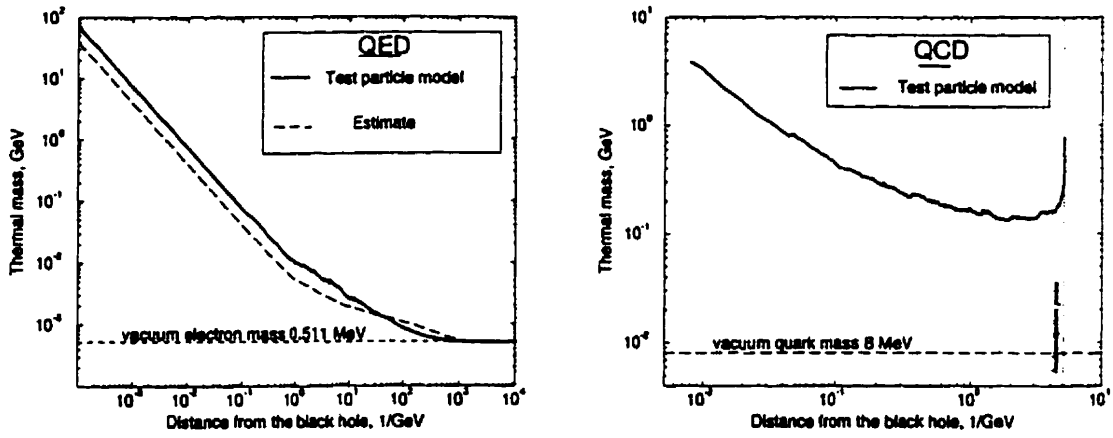

Figure 4.1: Thermal Mass in typical QED and QCD photospheres.

4.3 Bremsstrahlung Cross Section

The relativistic differential cross section for bremsstrahlung in the center of mass frame is [17, 18]

$$\frac{d\sigma(\omega)}{d\omega} \approx \frac{8\alpha r_e^2}{E\omega}\left(\frac{4}{3}(E-\omega)+\frac{\omega^2}{E}\right)\left(\ln\left[\frac{4E^2(E-\omega)}{m_e^2\omega}\right]-\frac{1}{2}\right), \tag{4.5}$$

where $\hbar = c = 1$, $r_e = \alpha/m_e$, E is the initial energy of each electron, and ω is the energy of the emitted photon. It diverges for $\omega \to 0$, but higher order corrections essentially impose an infrared cutoff [15].

The form of Eq. (4.5) suggests that lower energy photons are emitted more often, but considering the fact that they don't affect electron energy much, it is sensible to use the energy-averaged total cross section [15, 17]

$$\sigma = \int \frac{\omega}{E}\left(\frac{d\sigma}{d\omega}\right) d\omega \approx 8\alpha r_e^2 \ln\frac{2E}{m_e}. \tag{4.6}$$

Total photon-electron pair production cross section shows the same functional dependence in the extreme relativistic limit and we therefore use the same estimate (4.6) for both interactions. Fig. 4.2 will give an idea of how the cross section changes in a typical (QED) photosphere.

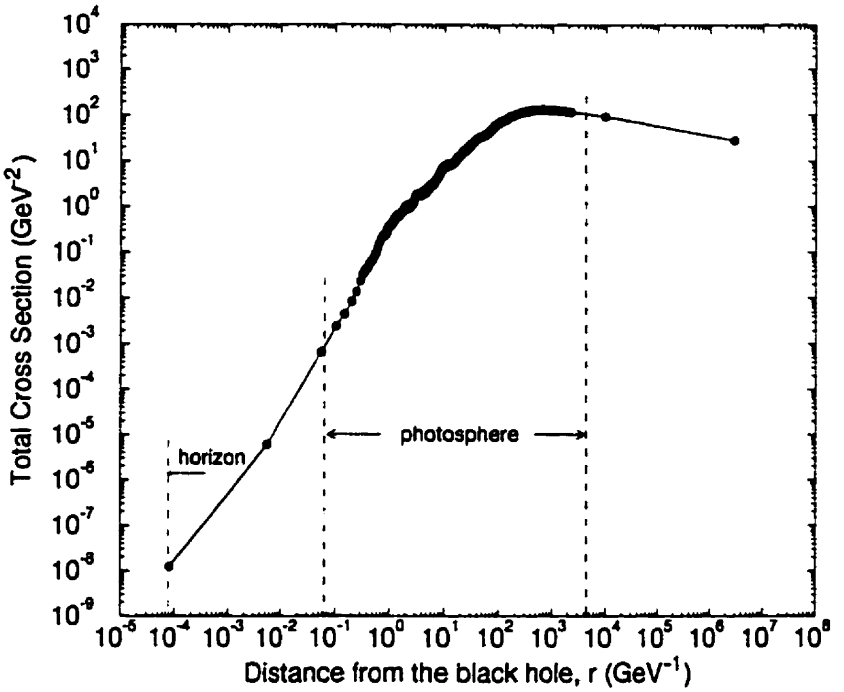

Figure 4.2: Total bremsstrahlung cross section σ in a typical QED photosphere ($T_{BH} = 1000$ GeV).

An improvement on the above treatment would be to use differential bremsstrahlung cross section and produce low energy photons with higher probability. However, one should then impose an infrared cutoff on the emitted photon energy and show that no meaningful physical properties of the photosphere depend on this cutoff.

4.4 Mean Free Path

The Boltzmann equation for the radial evolution of particle distribution [see Eq. (3.4)] will be equivalent to the usual time evolution version [see Eq. (3.1)] only when the

collision term is divided by the radial velocity factor v_r. Then the mean free path becomes

$$\lambda = \frac{1}{n(r)\langle v_{rel}\frac{\sigma}{v_r}\rangle}. \tag{4.7}$$

In our simulation, we do not need to do integrals to calculate the average quantity in the denominator, since the test particles are already distributed according to f and $\langle v_{rel}\sigma v_r^{-1}\rangle$ can simply be calculated as an average over the interacting pairs of test particles.

The mean free path can be estimated using Eq. (3.9) with $v_{rel} \simeq 1$ (see next section), σ from Eq. (4.6) and $n(r)$ from Eq. (3.14). We should not forget that m_e in these equation is the electron thermal mass [see Eq. (4.1)]. Combining all of these equations we get an estimate close to the one used by Heckler to characterize the photosphere:

$$\lambda = \frac{1}{n(r)\langle v_{rel}\frac{\sigma}{v_r}\rangle} \approx \frac{\pi}{8\alpha^2}\frac{N(r)/N(r_h)}{T_{BH}\ln(2E/m_e)}. \tag{4.8}$$

In Figure 4.3 we compare it to the mean free path calculated by direct evaluation of Eq. (4.7) in the test particle approach.

We see that the analytic estimate is in good agreement with the numerical result in the beginning and middle of the photosphere (and indeed we will see in Chapter 5 that Heckler's value for critical temperature is almost the same as ours), but they differ drastically in the end. His barely increasing mean free path lets the particles in the photosphere interact almost indefinitely, or rather until their average energy drops below m_{0_e}, when positrons and electrons annihilate. In contrast, the skyrocketing mean free path in our model means that when the radius becomes greater than $1/m_{0_e}$ ($r \sim 2 \times 10^3$ 1/GeV) the particles become virtually free. We use this as the criterion for the edge of the QED photosphere. To be precise, we consider the particles free when the mean free path on the next step is 2-3 orders of magnitude higher than on the previous one. This sudden increase in λ happens because the diameter of the particle distribution around the black hole exceeds the range of the bremsstrahlung interaction and then only the particles spatially close to each other can interact. At this point the relative velocity v_{rel} in Eq. (4.7) becomes approximately zero, since all particles are moving almost radially and the relative velocity of two particles that are spatially close to each other will be very small. However, in the estimate (4.8), used in ref. [15], this effect is neglected and v_{rel} is taken to be unity regardless of the distance from the black hole. We will discuss the range and relative velocity in the next section.

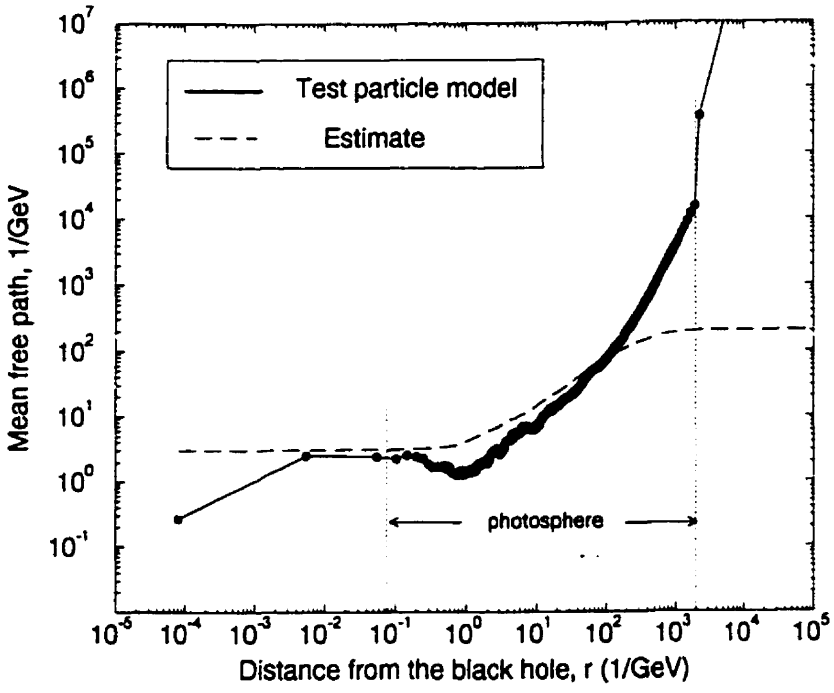

Figure 4.3: Mean free path λ in a typical QED photosphere ($T_{BH} = 1000$ GeV).

4.5 Interaction Distance and Relative Velocity

The distance at which particles can interact via bremsstrahlung and pair production is an important parameter, since we have to decide which test-particles may interact with one another and which may not. In the heavy ion collision problem, which was mentioned in the previous chapter as an example of using the test particle method, those test particles were allowed to interact which were within a critical distance, defined by $\sigma = \pi b_c^2$. We could use the same criterion: first find the average interparticle distance $b(r) = n(r)^{-1/3}$. As long as $b(r) < b_c$, we would randomly choose pairs of particles and assume that each pair consists of two nearest neighbors, position of which can be approximated by being at the same point. Since particle momenta are almost radial, the relative velocity of each pair is of order 0 and the mean free path calculated from Eq. (3.9) will increase extremely fast as a function of radius. Thus, no analog of photosphere can develop in this scenario.

However, the range of bremsstrahlung is somewhat higher than expected. Bremsstrahlung is conveyed by an exchange of a virtual photon. The range of the interaction is of order $1/k$ where k is the momentum of the virtual photon. It was shown in [20] that at relativistic energies, small momentum transfers, $k \simeq m_e$, contribute the bulk of the total cross section, therefore the distance at which particles

can interact via bremsstrahlung (and pair production) is of order $1/m_e$ (in plasma m_e is electron thermal mass).

This argument dramatically changes the value of average relative velocity. To see that, we should note that we are talking about microscopic black holes whose radii are of the same order as or smaller than the particle interaction distance. Specifically, for sufficiently high black hole temperatures, the horizon, $r_h \sim 1/T_{BH}$, happens to be lower than interaction range $1/m_e \sim 1/m_{pm}$. Moreover, we find that for some distance outward from the horizon, the plasma mass is decreasing significantly faster than the radius of the particle distribution is increasing. All this means that for certain black hole temperatures, all through certain radius away from the black hole any emitted particle can interact with any other *over the entire distribution*, which makes the average relative velocity of random interacting pairs of order 1. Fig. 4.4 shows how the distance of interaction remains higher than the radius of the particle distribution throughout the most of the photosphere.

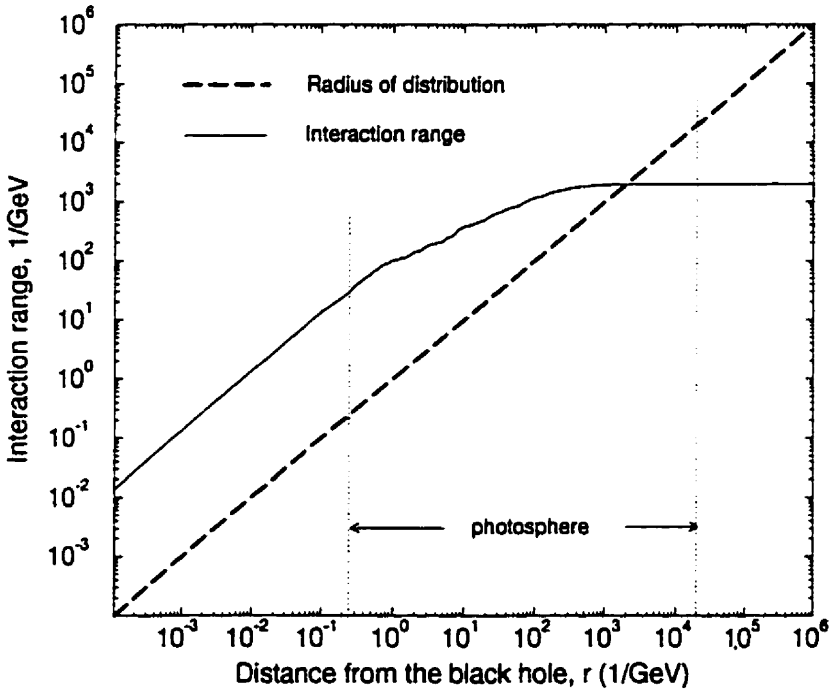

Figure 4.4: Minimum distance of interaction in a typical QED photosphere (T_{BH} = 1000 GeV).

Therefore, in our model we set $v_{rel} = 1$ as long as all the particles are capable of interacting with one another. However, when r becomes greater than the interaction range we use the procedure outlined at the beginning of the section and calculate relative velocity using the standard formula for highly relativistic particles:

$$v_{rel} \simeq \sqrt{2\left(1 - \frac{\mathbf{p}_1 \cdot \mathbf{p}_2}{p_1 p_2}\right)} \tag{4.9}$$

Next we must specify how the particle interactions are modeled. This is the subject of the next section.

4.6 Collisions

Before going into the details of collisions, we describe how the test particles are represented in the model. Each original and each newly created particle, be it photon or electron, is assigned an individual index i and ID number $ID(i)$, designating its spin. Each test particle has momentum, written in terms of its absolute magnitude (kinetic energy of the particle), $p(i)$, and two of its coordinates: radial, $p_r(i)$, and transverse, $p_t(i)$, (see Fig. 3.2). Although one of these three numbers is redundant, it is more convenient to keep it than recalculate it each time it is needed. On the other hand, azimuthal angle is not kept track of and is chosen at random when necessary.

In the algorithm for propagating test particles outlined in Section 3.5, the pairs after having been sorted by interaction probability (those with higher transverse momentum components are more likely to collide) are made to undergo actual collisions. We assume purely classical (except for creation of a third particle), three dimensional scattering which in principle should be straightforward, but in fact involves several subtleties in the context of our model.

First of all, as was shown in the previous section, most of the time the interacting particles can be at any two points on the radiation surface (surface of current radius r). Curiously, that means that two particles moving directly away from each other are as likely to interact as those that move directly towards each other. Secondly, if the pair consists of an electron and a photon we have to check that there is enough energy available to create two new electrons via pair production. We know that in the center of mass system all the available energy is distributed between the three new particles, so we transform the momenta of the pair to this system. We use the formulas from [21]. The velocity of center of mass frame is

$$\boldsymbol{\beta} = \frac{\mathbf{p}_1 + \mathbf{p}_2}{E_1 + E_2}; \tag{4.10}$$

the center of mass energy is

$$E_{cm} = \sqrt{(E_1 + E_2)^2 - (\mathbf{p}_1 + \mathbf{p}_2)^2}; \tag{4.11}$$

the momentum of one of the particles is

$$\mathbf{p}_{cm} = \gamma\left(\frac{\mathbf{p}_1 \cdot \boldsymbol{\beta}}{\beta} - \beta E_1\right)\frac{\boldsymbol{\beta}}{\beta} + \left(\mathbf{p}_1 - \frac{\mathbf{p}_1 \cdot \boldsymbol{\beta}}{\beta}\frac{\boldsymbol{\beta}}{\beta}\right) \tag{4.12}$$

and the momentum of the other is $-\mathbf{p}_{cm}$.

We must impose energy conservation,

$$2E_{cm} = E_1' + E_2' + E_3', \tag{4.13}$$

where E_1', E_2' and E_3' are the energies of the final particles. These energies are chosen randomly, but the respective momenta must satisfy momentum conservation, so the vectorial sum of the new momenta to be generated in the next step of the algorithm must be zero. The condition on the kinetic energy of each particle is found from geometrical considerations and turns out to be the triangle inequality:

$$|p_1' - p_2'| < |p_3'| < |p_1' + p_2'| \tag{4.14}$$

So far we have only distributed the energy, but have not assigned any momenta. We take these to have random directions in the CM frame. This assumption actually does not affect the evolution of the photosphere for radii smaller than the range of bremsstrahlung interaction. It does affect the sharpness of the outer edge of the photosphere, but this is already so sudden that using the true angular distributions of the differential cross section can have only a very small effect on our results.

We need to generate 9 momenta coordinates, but we know that the sum of the momenta is zero (3 equations) and we know their magnitudes (3 equations). We use two of the available degrees of freedom to to put all three vectors in x-y plane (set $z_1 = 0$ and $z_2 = 0$, the third vector will have to be in the same plane to satisfy conservation). Then we use one degree of freedom to put $\mathbf{p}_1$ along x-axis ($y_1 = 0$). We find the remaining coordinates of all three vectors in this specialized frame.

The next step is to rotate the plane containing the momentum vectors by three random Euler angles (θ, ϕ, ψ). We use matrix transformation (see, for example, [22])

$$\mathbf{p}' = \mathbf{A}\mathbf{p}, \tag{4.15}$$

where the matrix $\mathbf{A}$ is given by

$$\mathbf{A} = \begin{pmatrix} \cos\psi\cos\phi - \cos\theta\sin\phi\sin\psi & \cos\psi\sin\phi + \cos\theta\cos\phi\sin\psi & \sin\psi\sin\theta \\ -\sin\psi\cos\phi - \cos\theta\sin\phi\cos\psi & -\sin\psi\sin\phi + \cos\theta\cos\phi\cos\psi & \cos\psi\sin\theta \\ \sin\theta\sin\phi & -\sin\theta\cos\phi & \cos\theta \end{pmatrix}$$

Finally, by reversing $\boldsymbol{\beta}$ in Eq. (4.10) we get the three momenta back in the laboratory frame, where the new kinetic energy, and radial and transverse momenta are assigned to the new particles.

It should be noted, that even though the random choice of final energies (and directions) is somewhat less realistic than the more laborious procedure of weighting the possible final state configurations by the differential cross section, we estimate that it is justifiable, since soft bremsstrahlung photons which are more likely to be created would have but a small effect on the particle energy spectrum.

Chapter 5

QED Photosphere

In this chapter we will present the results of test particle modeling of black hole emission, considering only electrons, positrons and photons. This restriction is appropriate for black holes with $T_{BH} < \Lambda_{QCD}$. We will also treat higher temperatures in this context for the sake of understanding, deferring study of the effects of quarks and gluons until the next chapter. For the present, we determine under what conditions a dense, interacting plasma may be formed just considering QED. We will show the main characteristics of such photospheres for black holes of different masses and temperatures. Next, the momentum distributions inside of a typical photosphere will be explored. The last section will discuss the difference between the energy spectrum of the radiation at the horizon and at the edge of the photosphere, which is phenomenologically most relevant aspect of black hole photospheres.

5.1 Photosphere Formation

Armed with the model and algorithm of Chapter 3 and the calculation details of Chapter 4, we are ready to investigate the existence and properties of the photosphere suggested in Chapter 2. We fix the black hole temperature T_{BH} and allow the particles emitted from the Schwarzchild horizon with the Hawking energy spectrum to propagate outward, interacting via bremsstrahlung and photon-electron pair production. We confirm the formation of a photosphere for black hole temperatures $T_{BH} \sim 100$ GeV and higher. The photosphere first appears at a radius $r_0 \sim 10^2 - 10^3\, r_h$ (where $r_h = 1/4\pi T_{BH}$ is the Schwarzchild radius), and is characterized by a region of intense collisions terminating at a distance of $r_f \sim 10^7 - 10^8\, r_h$ from the black hole. The intensity of collisions is characterized by a very slow increase or even decrease of the mean free path in the photosphere compared to the interior and exterior regions (see Fig. 4.3).

The photosphere forms only for black holes above a certain critical temperature T_c. We adopt the same definition of T_c as was introduced by Heckler [15]. The idea is to define a quantity $\mathcal{N}(r)$ denoting the number of scatterings an average particle

undergoes between the horizon and some radius $r > r_h$. The criterion for having a photosphere is taken to be that on average every particle undergoes a collision at least once between leaving the horizon and escaping to infinity, in other words that

$$\lim_{r\to\infty} \mathcal{N}(r) \geq 1. \tag{5.1}$$

The critical black hole temperature is then the temperature of a black hole for which this limit is exactly unity.

Our numerical results for $\mathcal{N}(r)$ are shown for several black hole temperatures in (Fig. 5.1).

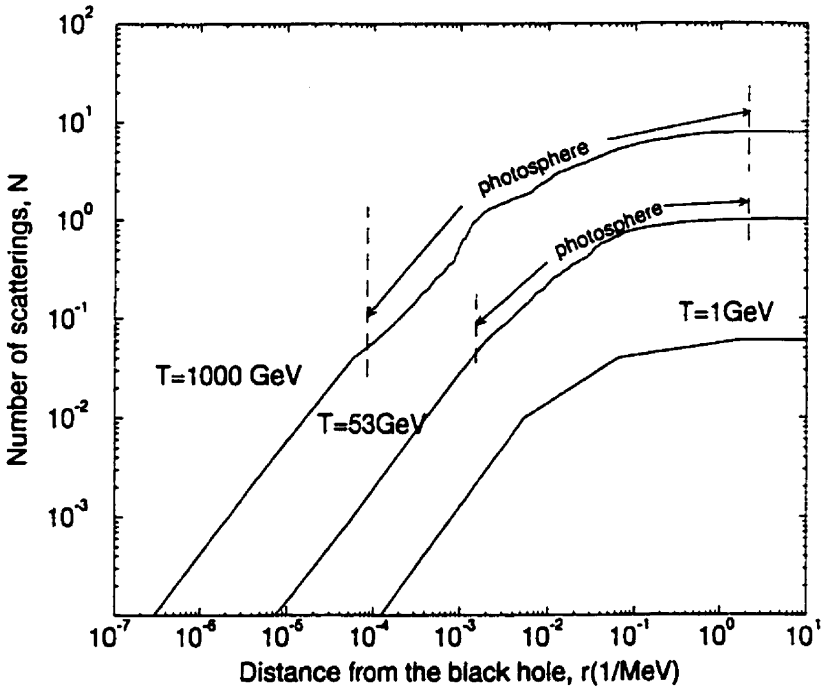

Figure 5.1: The number of scatterings an average particle undergoes between the horizon and radius r: $\mathcal{N}(r)$. The results are obtained from test particle model of emission; for numerical results by Heckler cf. Fig. 2.1.

The critical temperature we obtain is

$$T_c \simeq 50 \text{ GeV}. \tag{5.2}$$

It is of the same order of magnitude as that obtained in [15] by solving numerically Eq. (2.7): 45.2 GeV.

5.2 Photosphere Parameters

Here we will present the photosphere parameters obtained from simulations for approximately 30 different black hole temperatures. These parameters include the radii of the inner and outer surfaces, $r_0(T_{BH})$ and $r_f(T_{BH})$ respectively, the total particle production factor $P(T_{BH})$ and the average energy of the particles emerging from the photosphere $\overline{E}_{edge}(T_{BH})$. The latter is relevant because it is the average energy of particles that may eventually reach a distant observer. We will point out large discrepancies between these results and the fluid model used in [15] (Chapter 2), and derive empirical formulas for r_0, r_f and $\overline{E}_{edge}$ from our data.

Inner radius

To define the inner radius, we use the fact that in our model, particles propagate over discrete distances Δr which are fractions of the mean free path (see p.15). For $T_{BH} \ll T_c$ the mean free path changes by several orders of magnitude at each step and we can say that particles are streaming virtually free to infinity. For $T_{BH} \gtrsim T_c$ this happens for the first several steps, but then the mean free path abruptly levels off. We define the beginning of the photosphere for at a radius, where two subsequent mean free paths are of the same order of magnitude, or equivalently, when

$$\frac{\lambda_{i+1}}{\lambda_i} \sim \frac{\lambda_i}{\lambda_{i+1}} \quad \left(\leftrightarrow \frac{\Delta r_{i+1}}{\Delta r_i} \sim \frac{\Delta r_i}{\Delta r_{i-1}} \right), \tag{5.3}$$

then $r_0 \equiv r_i$.

We find that r_0 is usually three steps away from the horizon ($i = 3$). The values of r_0 in units of $1/\text{GeV} \simeq 0.197$ fm are plotted in Fig. 5.2 as a function of black hole temperature. As one can see from the graph, r_0 decreases with the temperature and can be very closely fitted by

$$r_0 = \frac{1}{\kappa T_{BH}}, \quad \text{where } \kappa = 0.01800 \pm 0.00004. \tag{5.4}$$

We know that the radius of the Schwarzchild horizon is also inversely proportional to the black hole temperature $r_h = 1/4\pi T_{BH}$, so that

$$r_0 = \frac{4\pi}{k} r_h \simeq 698\, r_h. \tag{5.5}$$

By this criterion, the photosphere starts to develop much closer to the black hole than was predicted ($r_0 \sim 10^9 r_h$) in [15] using a fluid model for the interacting particles.

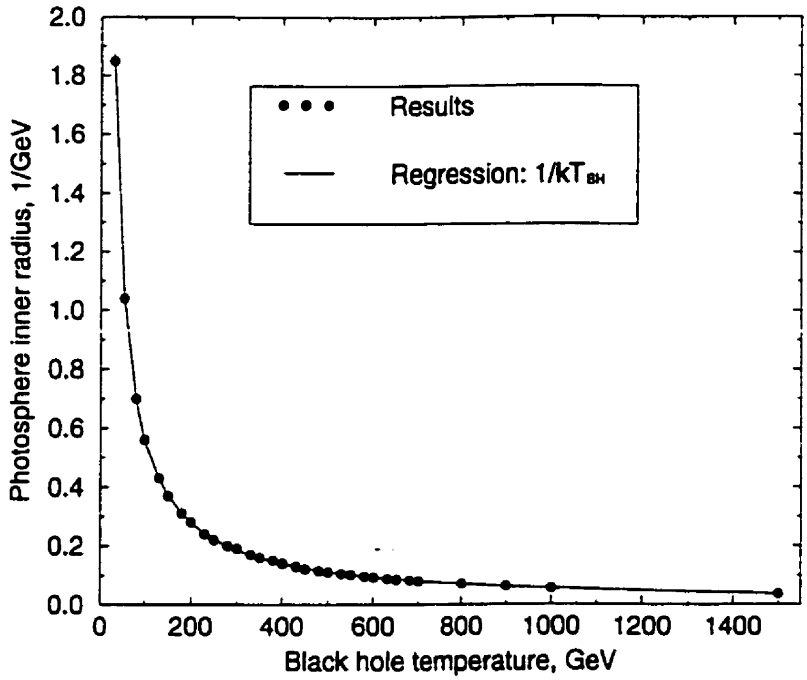

Figure 5.2: Radii of inner photosphere surface for different black hole temperatures (black dots). Solid line represents inverse regression over these values, see Eq. (5.4).

Edge Radius

The outer radius of the photosphere, r_f, can be defined similarly to the inner, except that the next mean free path should be much bigger than the previous one,, when

$$\frac{\lambda_{i+1}}{\lambda_i} \gg \frac{\lambda_i}{\lambda_{i-1}} \tag{5.6}$$

then $r_f \equiv r_i$.
This radius is easily found in practice because the next step after r_f is usually several orders of magnitude larger, implying that the particles have become virtually free. For the same reason, r_f was not precisely determined and a refined algorithm making the steps smaller near the edge of the photosphere will be used in future work. The precision in r_f is not essential, however, because it is not an observable quantity, and hence this refinement will have no effect on average particle energy at the edge.

In the present model r_f remains in the same range for all black hole temperatures shown and the only correlation that can be inferred is that the dispersion of values decreases with rising temperature (Fig. 5.3). We can interpret these results as disper-

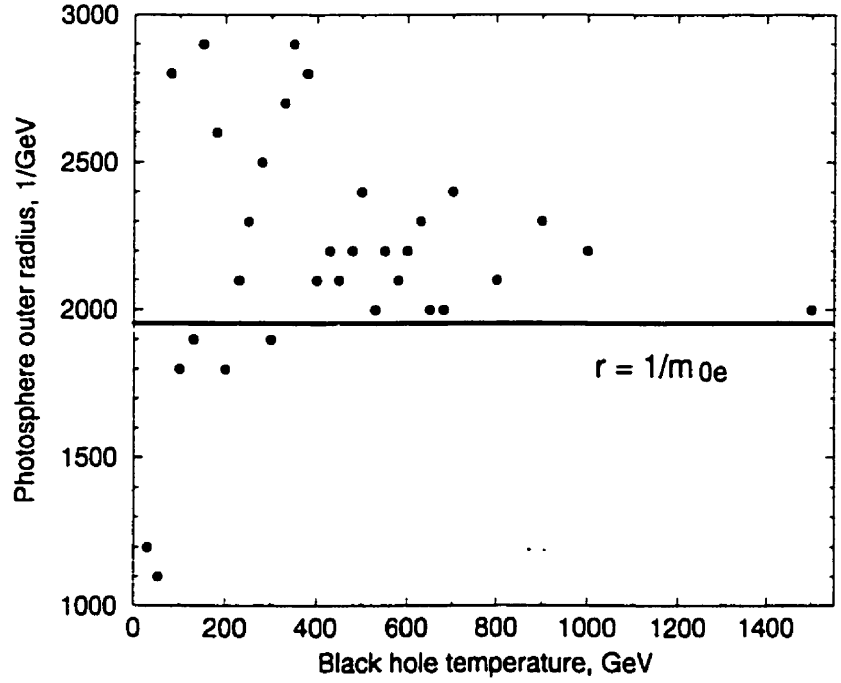

Figure 5.3: Radii of outer photosphere surface for different black hole temperatures (black dots). Solid line represents $r = 1/m_{0_e}$, radius where particles can no longer interact all over the black hole.

sion around a constant value of $r \sim 2000$ 1/GeV, which is close to $1/m_{0_e}$. But $1/m_e$ is the range of bremsstrahlung interaction. We showed (see p. 24) that once the radius of the particle distribution exceeds this value, particles can no longer interact with all the others around the black hole and we then have to assume that the interaction is between nearest neighbors. The relative velocity between interacting particles then drops sharply from ~ 1 to ~ 0 (since the particles move almost radially) and with it the interaction rate $\Gamma \sim n\langle v_{rel}\sigma\rangle$. This marks the end of the photosphere.

The dispersion of values of r_f for different black hole temperatures can be explained by the discreteness of steps in the model. In fact, the higher the temperature, the finer are the steps all over the photosphere, since the mean free path is shorter, and we take Δr to be $\lambda/50$.

Particle Production

Another useful parameter for characterizing the photosphere is total particle production factor, given by:

$$P = \frac{N(r_f)}{N(r_h)}, \tag{5.7}$$

where $N(r)$ is the number of test particles at radius r. P can be used to quantify the probability of interactions inside the photosphere, since at each collision $N \to N+1$. Figure 5.4 shows P as a function of black hole temperature. We find that it can be

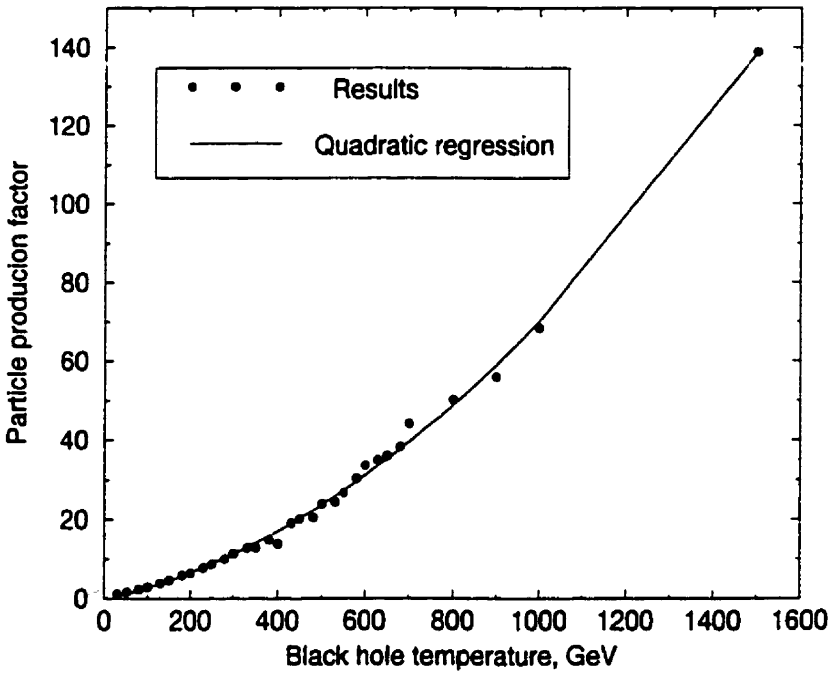

Figure 5.4: Particle production factor $N(r_f)/N(r_h)$ for different black hole temperature. Solid line is quadratic regression of the results [see Eq. (5.8)].

represented by a quadratic fit (solid line):

$$P(T_{BH}) \simeq bT_{BH} + cT_{BH}^2, \tag{5.8}$$

where $b = 0.026\ \text{GeV}^{-1}$ and $c = 4.5 \times 10^{-5}\ \text{GeV}^{-2}$. The dominant quadratic term suggests that photospheres become very dense in the last stages of black hole evaporation.

Average Final Energy

From an observational point of view, the reduction in average energy of emitted particles is one of the most relevant consequences of the photosphere. At the horizon,

$\overline{E}$ is approximately $3T_{BH}$. But the photosphere can reduce this number dramatically, so that a distant observer sees a much softer spectrum. The results are displayed in Figure 5.5.

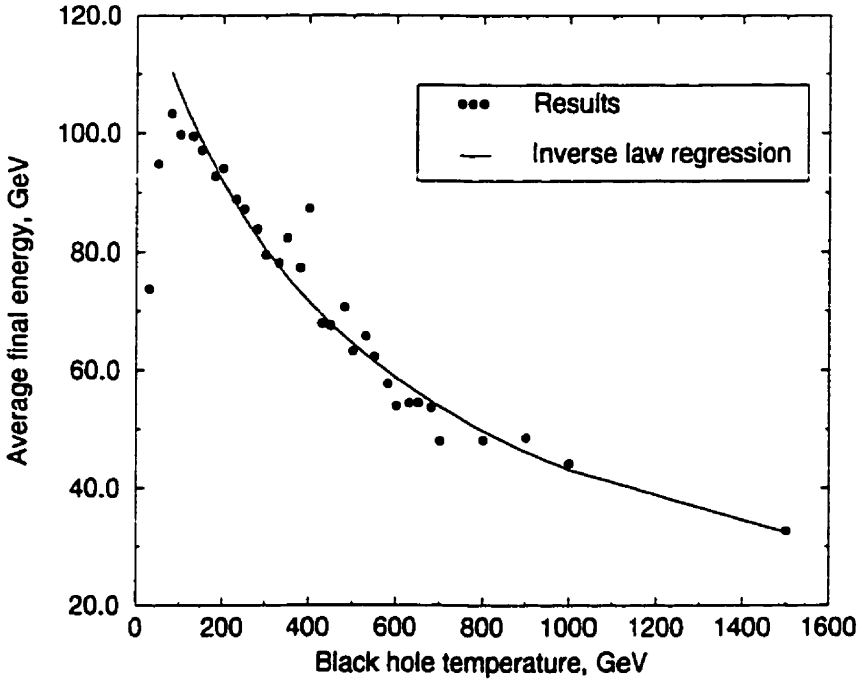

Figure 5.5: $\overline{E}_{edge}$ for different black hole temperatures.

We can compute $\overline{E}_{edge}$ from $\overline{E}_i$ and particle production factor, Eq. (5.8):

$$\overline{E}_{edge} = \frac{\overline{E}_i}{P} \simeq \frac{3T_{BH}}{bT_{BH} + cT_{BH}^2},$$

to obtain

$$\overline{E}_{edge} = \frac{3}{b + cT_{BH}}. \tag{5.9}$$

In the limit of high black hole temperatures ($b \ll cT_{BH} \Leftarrow T_{BH} > 10^4$ GeV):

$$\overline{E}_{edge} \simeq 6.7 \times 10^4 \frac{\text{GeV}^2}{T_{BH}} \tag{5.10}$$

This is a remarkable result since it predicts that for black holes of temperature $T_{BH} \gtrsim 100$ GeV ($M < 10^{12}$g) the effective temperature of emitted particles (the

one that could be observed far away from the hole) is actually the lower the higher is their temperature. For an individual black hole, which is losing mass and hence becomes hotter, this means that its effective temperature nevertheless goes down.

Of course, Eq. (5.10) is true only as long as our model is valid, and we assumed that black hole should not change much on the time scale of particle travel time from the horizon to the edge of the photosphere. Nevertheless, we expect the qualitative picture to be the same even for black holes temperatures above this limit of validity.

An overall picture of an individual black hole developing with time in view of the results of this section is as follows. As far as only QED emission is concerned, a photosphere starts to develop around the black hole when it evaporates to $M \simeq 5 \times 10^{12}$. At this point its effective temperature instead of going up inverse proportionally to its mass, levels off and begins to decrease. On the other hand, luminosity must go up to have energy conservation. Thus, it is not radiating like a black body. The outer edge of the photosphere remains at a radius of $400fm \sim 1/m_e$. However, its inner radius, $r_0 \sim 700\, r_h$, shrinks with the Schwarzchild horizon r_h. Eventually, if the steady state model is valid at these temperatures, the edge will cool to $\overline{E}_{edge} = m_{0_e}$, at which point the positrons and electrons will annihilate and no further cooling will occur. At this point, however, the black hole will be within 10^{-10} second of its total evaporation.

To give an idea of how the parameters obtained from test particle method differ from the estimates in [15] for which a non-perfect fluid model was used, we tabulate the relevant quantities analogously to table 2.2 to which it should be compared.

T_{BH}	r_0	$r_{edge}\,(r_f)$	$E_{avr}\,(\overline{E}_{edge})$
45 GeV	1.23 GeV^{-1}	1.5×10^3 GeV^{-1}	90.1 GeV
300 GeV	0.19 GeV^{-1}	1.9×10^3 GeV^{-1}	79.5 GeV
1000 GeV	5.56×10^{-2} GeV^{-1}	2.2×10^3 GeV^{-1}	44.2 GeV

Table 5.1: QED photosphere parameters for several black hole temperatures obtained in test particle simulation.

5.3 Inside the Photosphere

A more detailed picture of the plasma can be gotten from the particle momenta distributions at different radii. Since no significant interactions start before $r =$

$10^2 - 10^3 r_h$, particles move increasingly radially until the inner boundary of the photosphere. Then they start interacting with one another and their momenta become more thermalized. Close to the end of the photosphere, the mean free path increases so that particles again increase the radial components over the growing mean free path. These developments can be seen in the distribution of $p_t/p = p_t/\sqrt{p_t^2 + p_r^2}$ for several radii inside a photosphere, in Figure 5.6. (When $p_t/p \simeq 0$, the particle moves almost radially outward; if $p_t/p \simeq 1$ it would move perpendicularly to the radial direction.)

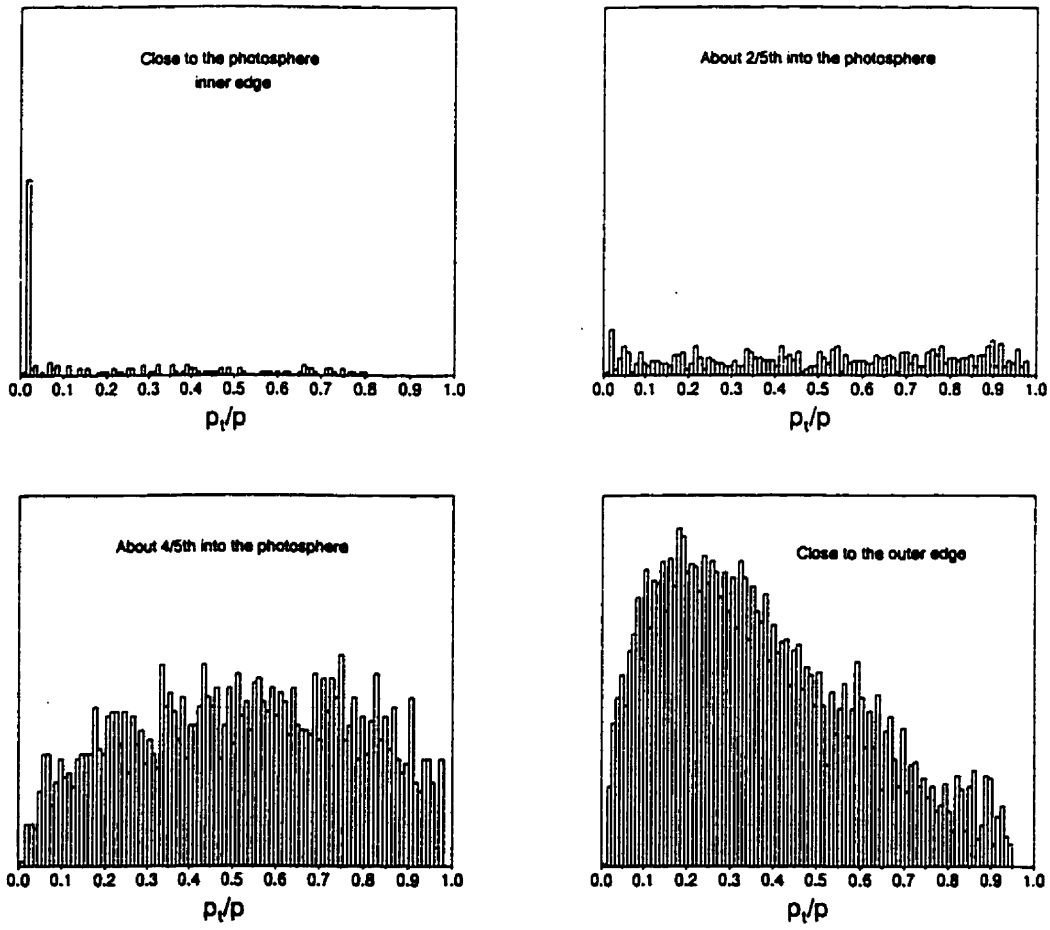

Figure 5.6: Distribution of p_t/p for several radii in the photosphere of a 1000 GeV black hole.

5.4 Spectra

Finally, we examine the detailed particle energy spectra at the black hole horizon and at the photosphere edge (Fig. 5.7). The shift towards the lower energies is the most

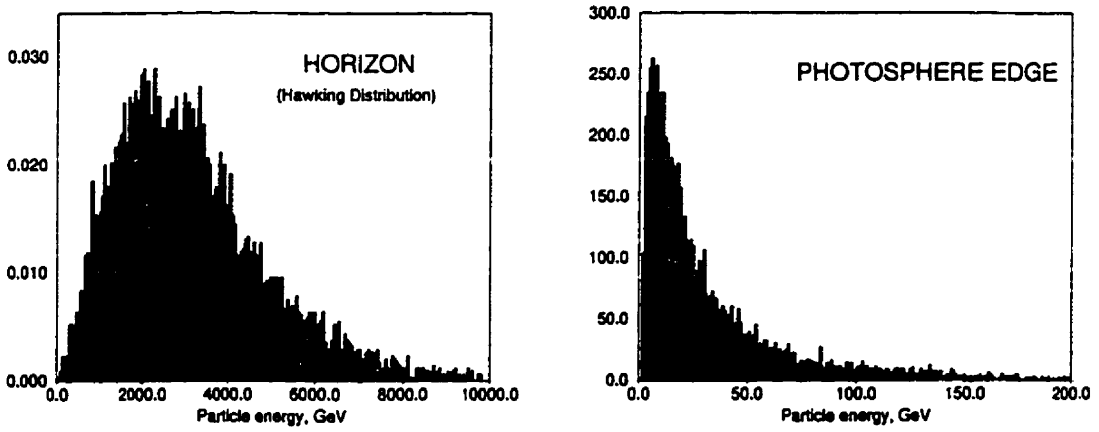

Figure 5.7: Energy spectrum of a 1000 GeV (10^{11}g) black hole at the Schwarzchild horizon and near the edge of the photosphere.

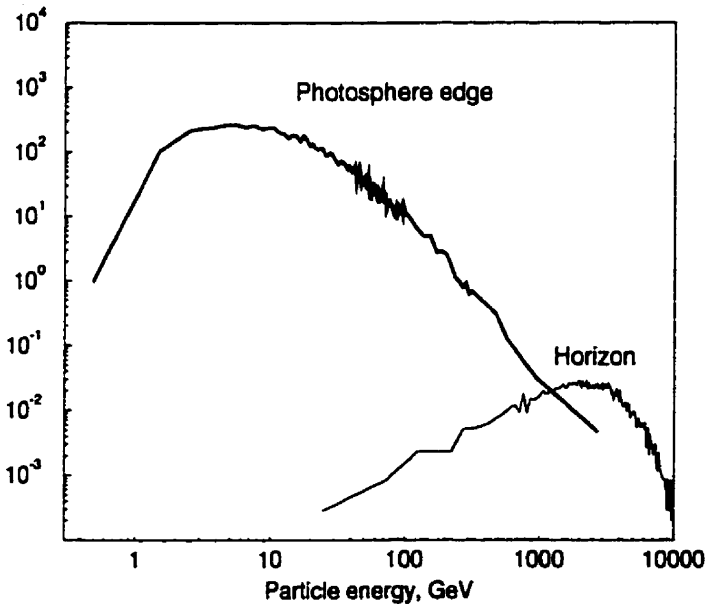

Figure 5.8: Energy spectrum of a 1000 GeV (10^{1}1g) black hole at the Schwarzchild horizon and near the edge of the photosphere.

significant difference between the original distribution at the horizon and those within the photosphere. The two are shown together in figure 5.8, where it can be seen that the softening in energy is accompanied by an increase in the number of particles, as is required by energy conservation.

The QED photosphere by itself serves as a kind of toy model for the real black holes, which are also emitting quarks and gluons at the temperatures we are considering. We now turn our attention to the QCD photosphere.

Chapter 6

QCD Photosphere

This chapter will discuss another part of the spectrum of particles emitted by microscopic black holes. A black hole whose temperature exceeds $\Lambda_{QCD} \sim 200$ MeV, i.e., a black hole with mass $M_{BH} \lesssim 5 \times 10^{14}$ g, emits quarks and gluons which, as proposed by MacGibbon and Weber in [12] fragment into hadrons, decaying in their turn into stable particles. We will model the interactions of the quarks and gluons before fragmentation takes place. At this stage, as suggested by Heckler in [15], a quark-gluon photosphere analogous to the electron-photon photosphere in QED may develop, changing the energy spectrum of the particles. In Section 1 we will see how the test particle method was applied in the QCD case. Then we will look at the parameters of the QCD photosphere for different black hole temperatures and see how the energy spectrum of quarks and gluons changes between the time of emission from the horizon and the moment of hadronization (Section 2). Section 3 will deal with the hadronization process, and we will derive the energy distribution of photons produced in pion decay on the edge of the photosphere and compare it to the distributions obtained for the same black hole when the photosphere is neglected.

6.1 Test Particle Method in QCD

Our treatment does not attempt to give a detailed model of QCD interactions after hadronization begins. However, the onset of the photosphere can be established in terms of free quarks and gluons interacting with each other. We assume that hadronization occurs at a distance of $\sim \Lambda_{QCD}^{-1}$ and that no significant softening of the particle spectrum occurs after this point. Hence, we make the same test particle simulation as in QED, only with different interaction cross section, masses, and number densities. Due to the much larger coupling constant and greater number of degrees of freedom, we expect the photosphere to develop at temperatures $T_{BH} \ll T_c^{QED} \sim 50$ GeV, and to reach higher density than in the QED case.

To investigate the photosphere in QCD, we recall that the key issue was the inclusion of $2 \rightarrow 3$ body interactions in the collision term of the Boltzmann

equation (3.4). Like electrons and photons, quarks and gluons can also interact via bremsstrahlung ($q + q \to q\,q\,g$) and pair production ($q + g \to q\,q\,\bar{q}$). The relevant diagrams are

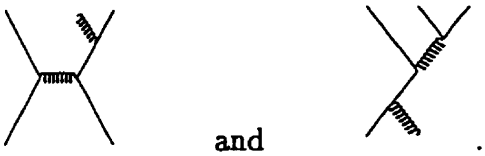

and

We estimate that other diagrams, as, for example, for pair production

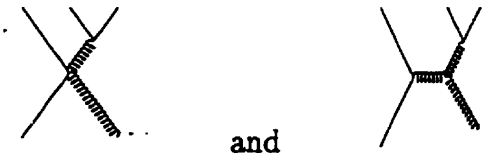

and

are less important since they don't have the almost on-shell quark propagator and the gluon thermal mass is subdominant.

To simplify matters, we will use the same form of cross section as in QED [see Eq. (4.6)], changing fine structure constant α into strong coupling constant α_s and electron mass into quark mass:

$$\sigma_{brem}^{QCD} \simeq \frac{8\alpha_s^3}{m_q^2} \ln \frac{2E}{m_q}. \tag{6.1}$$

By m_q we mean the quark thermal mass. Using the same approximations as in QED (see Section 4.2) we estimate that

$$m_q(r) \simeq \sqrt{m_{0_q}^2 + 4\pi\alpha_s \left(\frac{1}{2} n_q \left\langle \frac{1}{p_q} \right\rangle + n_g \left\langle \frac{1}{p_g} \right\rangle \right)}, \tag{6.2}$$

where m_{0_q} is quark vacuum mass, n_q and n_g are densities of quarks and gluons, and averages of $\langle p_q^{-1} \rangle$ and $\langle p_g^{-1} \rangle$ are taken over the test-quarks and test-gluons.

Because the bremsstrahlung cross section goes like $1/m_q^2$, of all the quarks we assume that only the two lightest ones and their antiquarks are relevant and hence for quark vacuum mass we use the average value $m_{0_q} = 8$ MeV. How quark thermal mass changes with radius in a typical QCD photosphere was shown on Fig. 4.1. As a matter of fact, since the thermal mass is significantly greater than vacuum mass everywhere in the photosphere, for higher black hole temperature we should also include into consideration heavier quark species (s,c and b, as well as their antiquarks,

for $T_{BH} \gtrsim 5$ GeV). This work is now in progress. We estimate, however, that it will not significantly change the picture of the QCD photosphere. Our present results represent the lower bound on the photosphere parameters.

Unlike in QED, the coupling constant in the two equations above depends strongly on energy. To leading order in perturbation theory [23]:

$$\alpha_s(\mu) = \frac{12\pi}{(33 - 2n_f)\ln\left(\mu^2/\Lambda^2_{QCD}\right)}, \tag{6.3}$$

where in the model we take μ to be average particle energy at a given radius, $n_f = 4$ (number of relevant quarks and antiquarks) and $\Lambda_{QCD} \sim 200$ MeV.

We have to remember that when the temperature of the quark-gluon plasma approaches Λ_{QCD}, perturbation theory in α_s is no longer valid, and in fact at this point quarks and gluons will form hadrons. This process will be discussed in Section 4. The radius where this happens naturally defines the photosphere outer edge, because even though the interactions still take place after hadronizaton, by comparing the mean free path of the hadrons to the life-time of unstable pions we conclude that strong interactions quickly shut off.

The density of particles should include QCD degrees of freedom. For quarks: 4 kinds of quarks $(u, \overline{u}, d, \overline{d})$ $\times$ 3 colors; for gluons: 8 gluon colors. Eq. (3.14) becomes

$$n_{QCD}(r) = \frac{\zeta(3)}{\pi^2(4\pi)^2}\frac{T_{BH}}{r^2}\begin{cases} 18\Gamma_f\, R_f(r) & \text{for fermions} \\ 16\Gamma_b\, R_b(r) & \text{for bosons,} \end{cases} \tag{6.4}$$

where $R_{f(b)}(r)$, as defined in Eq. (3.13), account for the creation of new fermions and bosons. With these changes to the formulas of Chapters 4 and 5 we have modeled the quark-gluon plasma around black holes and the results are given in the following sections.

6.2 Parameters of QCD Photosphere

We have found that the QCD photosphere starts to develop for all black hole temperatures higher than

$$T_c^{QCD} \simeq 175 \text{ MeV}. \tag{6.5}$$

This is more than two orders of magnitude lower than the critical temperature for the QED photosphere. It also agrees with the analytical estimate in [15], $T_c^{QCD} \sim \Lambda_{QCD}$.

However, we have to note that the value for critical temperature (6.5) is defined by $\mathcal{N}(r_f) \simeq 1$ and not by the limit $\lim_{r\to\infty}\mathcal{N}(r)$ which simply does not exist (see

Fig. 6.1). This value is slightly higher than $T_{BH} = \Lambda_{QH}$, temperature at which a black hole starts to emit quarks and gluons. Comparing the graphs of $\mathcal{N}(r)$ in Fig. 6.1 to

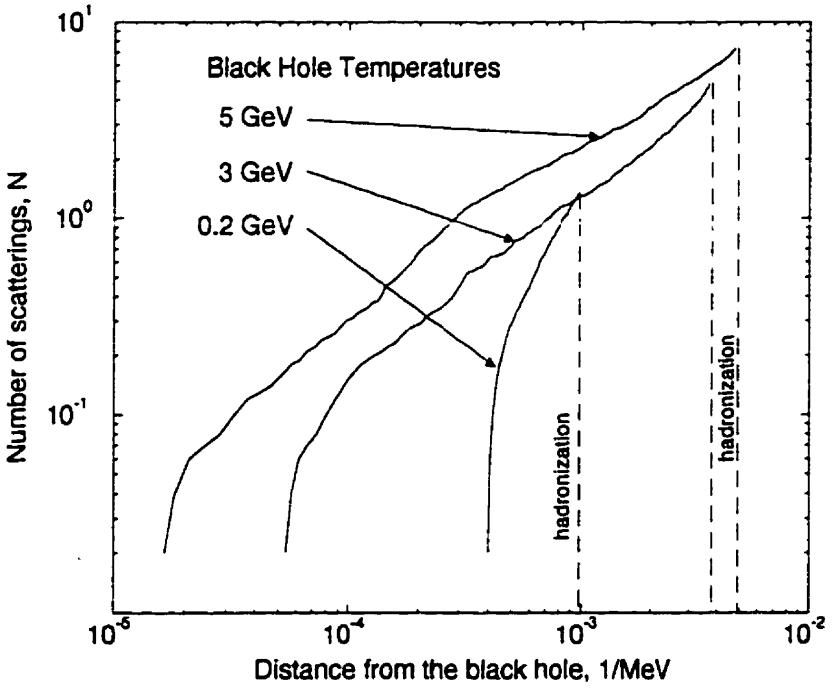

Figure 6.1: Average number of scatterings $\mathcal{N}$ in QCD photosphere as a function of radius r for several black hole temperatures. Note the differences with the analogous graph in QED (fig. 5.1).

Fig. 5.1 we can see that while in QED there is a clear dissipation of the photosphere, in QCD the steady increase in the number of scatterings is apparently checked only by hadronization.

Next, it is interesting to know the photosphere dimensions, particularly, the radii of its inner and outer surfaces. For the radius of the inner surface we cannot use the criterion described in Section 5.2 [see Eq. (5.3)], since it turns out that this surface is very close to the horizon. The physics in this region is more complicated than our model is designed to cope with (gravitational effects have to be taken into account) so we leave this issue open, taking note that significant interactions start close to the black hole horizon.

The radius of the outer surface, however, is well defined as the radius where hadronization takes place. Different conditions can be used to set the hadronization point: on interparticle spacing ($b = n^{-1/3} > 1/\Lambda_{QCD}$), on the average particle energy ($\overline{E} \sim \Lambda_{QCD}$) or on the coupling constant ($\alpha_s \gtrsim 1$). All three are roughly equivalent and the value of r_f depends only marginally on which one is actually used. In the

results shown in Fig. 6.2 the last criterion is used. Empirically, our results are well fit

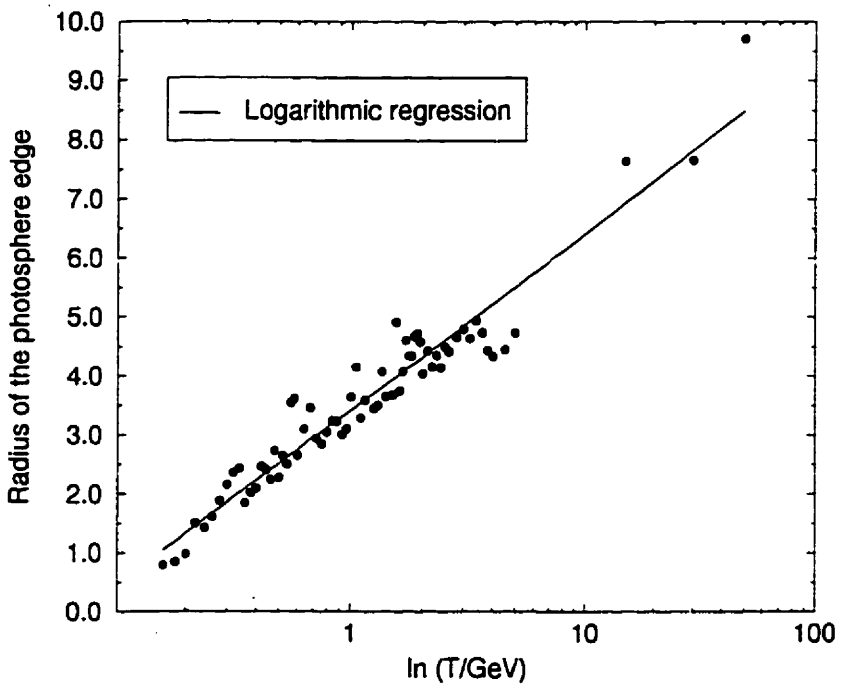

Figure 6.2: Radius of the outer surface of QCD photosphere versus logarithm of black hole temperature. This is the radius, where $\overline{E} \sim \Lambda_{QCD}$ and quarks and gluons form hadrons.

by a logarithmic growth in the photosphere radius with the black hole temperature:

$$r_f^{QCD} = A + B \ln\left(\frac{T_{BH}}{1\ \text{GeV}}\right), \tag{6.6}$$

where $A = 3.25 \pm 0.09\ \text{GeV}^{-1} \simeq 0.65$ fm and $B = 1.45 \pm 0.06\ \text{GeV}^{-1} \simeq 0.29$ fm.

The parameter which best shows the intensity of interactions in a QCD photosphere is total particle production factor $P(T_{BH}) = N(r_f)/N(r_h)$. As shown in Fig. 6.3, we find that it increases linearly with black hole temperature:

$$P^{QCD}(T_{BH}) = (8.62 \pm 0.01)\frac{T_{BH}}{\text{GeV}}. \tag{6.7}$$

Thus, the big picture of black hole evolution, in the light of the QCD photosphere, is as follows. A black hole that has reached a temperature greater than $\Lambda_{QH} \sim \Lambda_{QCD}$

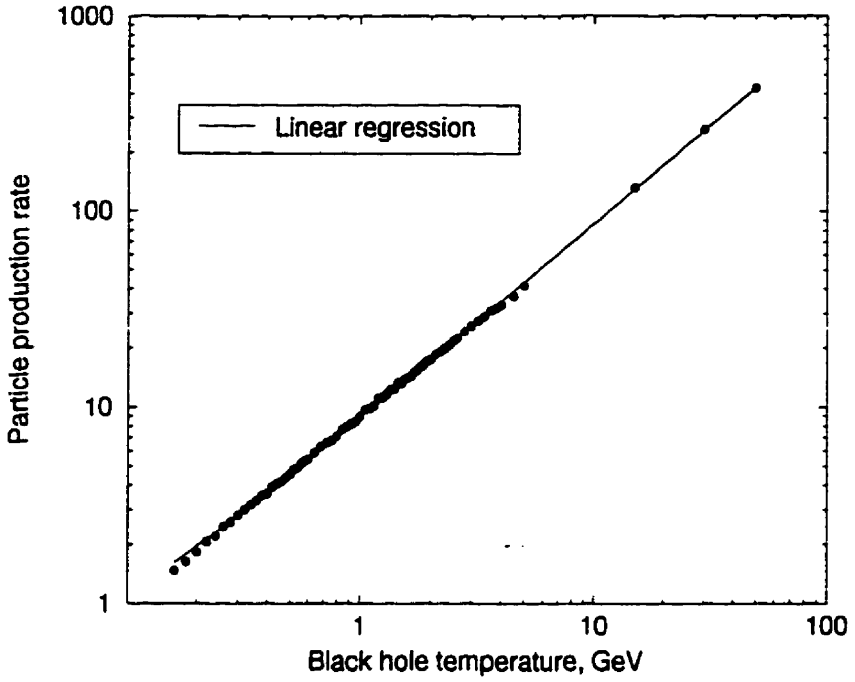

Figure 6.3: Total particle production in QCD photosphere vs. black hole temperature.

corresponding to a black hole mass of $M \lesssim 5 \times 10^{14}$ g emits quarks and gluons which almost immediately begin interacting to form a photosphere very close to the horizon $r_h \lesssim 0.08$ fm. As the black hole temperature continues to rise, photosphere inner radius shrinks along with the horizon ($r_0 \sim r_h \propto 1/T_{BH}$). Particles emitted from the horizon with average energy $\overline{E}_i \sim 3T_{BH}$ get processed in the photosphere and new particles are created. The higher the black hole temperature, the more particles are created (see Fig. 6.3). The average particle energy decreases as they propagate outward, until it reaches $\overline{E}_f \sim 300$ MeV on the photosphere edge, where hadronization occurs. The radius of the edge increases logarithmically [see Eq. (6.6)] with the black hole temperature.

The results are summarized in Table 6.1 in the form of the photosphere parameters for several characteristic black hole temperatures.

As we can see, the average particle energy can decrease by several orders of magnitude in a QCD photosphere. No less interesting is to know how the detailed spectrum changes. On Figure 6.4 we compare the energy distributions of the particles at the horizon and at the photosphere edge of a 1.5 GeV black hole. We see a very significant shift towards the lower energy end of the spectrum (cf. Fig 5.7) and an order of magnitude increase in the number of particles, which corresponds to

T_{BH}	$r_0 \sim r_h$	$r_{edge}\,(r_f)$	$\overline{E}_i$	$\overline{E}_{edge}$
200 MeV	0.4 GeV^{-1}	0.97 GeV^{-1}	600 MeV	300 MeV
1 GeV	0.08 GeV^{-1}	3.64 GeV^{-1}	3.0 GeV	300 MeV
50 GeV	0.0016 GeV^{-1}	9.74 GeV^{-1}	156 GeV	300 MeV

Table 6.1: QCD photosphere parameters for several black hole temperatures obtained from the test particle simulation.

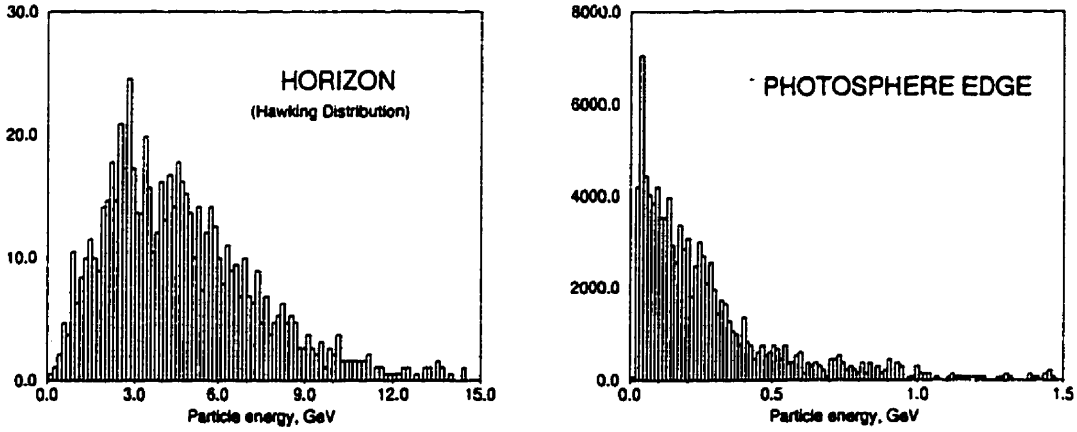

Figure 6.4: Energy distribution of quarks and gluons at the horizon of a 1.5 GeV black hole and at the edge of the photosphere

$P(1.5\ \text{GeV}) \simeq 13$ [see Eq. (6.7)]. However, quarks and gluons, whose distribution is presented in Fig. 6.4, do not reach a distant observer, but rather produce hadrons, the decay products of which could be observed far away from the black hole. Let us turn to the question of how to estimate the spectrum of these asymptotic particles, in particular photons, from the quark-gluon distribution at the edge of the photosphere.

6.3 Hadronization and Final Spectrum

Roughly speaking, the QCD interaction is perturbative ($\alpha_s < 1$) when the distance between the particles is smaller than Λ_{QCD}^{-1}. This condition is satisfied in the photosphere region. At larger distances, however, vacuum fragmentation of quarks and gluons will become dominant, which is what happens at the photosphere edge. For an accurate calculation of the spectrum of the photons which emerge after the hadrons

decay we would have to use the quark and gluon distributions at the edge of the photosphere and a jet fragmentation code for the final distributions of pions and photons [12, 24]. However, we can estimate this spectrum (within a factor of order unity [24]), with some sacrifice in accuracy, as a convolution of the quark-gluon spectrum, available from our test particle simulation, with the pion fragmentation function [2, 12] and the Lorentz-transformed spectrum of photons from π^0 decay [15]:

$$\frac{dN_\gamma}{dE_\gamma} = \int_{E_0}^{\infty} dE_\pi \, \frac{dg_{\pi\gamma}(E_\pi)}{dE_\gamma} \frac{dN_\pi}{dE_\pi}, \tag{6.8}$$

where $E_0 = E_\gamma + m_\pi^2/4E_\gamma$. The number of photons of energy E_γ created by a pion moving with velocity β and decaying isotropically in its rest frame is

$$\frac{dg_{\pi\gamma}(E_\pi)}{dE_\gamma} = \frac{2}{\gamma m_\pi \beta} = \frac{2}{\sqrt{E_\pi^2 - m_\pi^2}}, \tag{6.9}$$

where $\gamma = (1-\beta^2)^{-1/2}$. The pion spectrum is [12]

$$\frac{dN_\pi}{dE_\pi} = n_j \int_{E_\pi}^{\infty} dQ \, \frac{dg_{j\pi}(Q, E_\pi)}{dE_\pi} \frac{N_j}{dQ}, \tag{6.10}$$

where n_j, the number of QCD degrees of freedom available at the edge of the photosphere, equals to (3 quark colors $\times$ 4 relevant quarks) plus 8 gluon colors, in total $n_j = 20$. For the relative number of pions with energy E_π produced by each quark or gluon j we use [2]

$$\frac{dg_{j\pi}(Q, E_\pi)}{dE_\pi} = \frac{15}{16} \sqrt{\frac{Q}{E_\pi^3}} \left(1 - \frac{E_\pi}{Q}\right)^2. \tag{6.11}$$

Finally, dN_j/dQ is the quark-gluon distribution at the outer edge of the photosphere.

Combining 6.8 through 6.11 we obtain the final convolution double integral:

$$\frac{dN_\gamma}{dE_\gamma} = \int_{E_0}^{\infty} dE_\pi \, \frac{2}{E_\pi^{3/2}\sqrt{E_\pi^2 - m_\pi^2}} \int_{E_\pi}^{\infty} dQ \, \frac{20 \times 15}{16} \sqrt{Q} \left(1 - \frac{E_\pi}{Q}\right)^2 \frac{dN}{dQ}, \tag{6.12}$$

where $E_0 = E_\gamma + m_\pi^2/4E_\gamma$.

We have calculated the integral 6.12 numerically for several black hole temperatures. The results for one of them ($T_{BH} = 50$ GeV) are presented in Fig. 6.5 and compared to the results obtained neglecting the photosphere, but taking into account

direct quark fragmentation at the photosphere horizon and subsequent π^0 decay (as in [12]). Also shown are the spectrum of photons emitted directly from the black hole (neglecting the QED photosphere) and from the QED photosphere, which just starts to form at this temperature. The actual full spectrum of a 50 GeV black hole is the addition of the two solid lines.

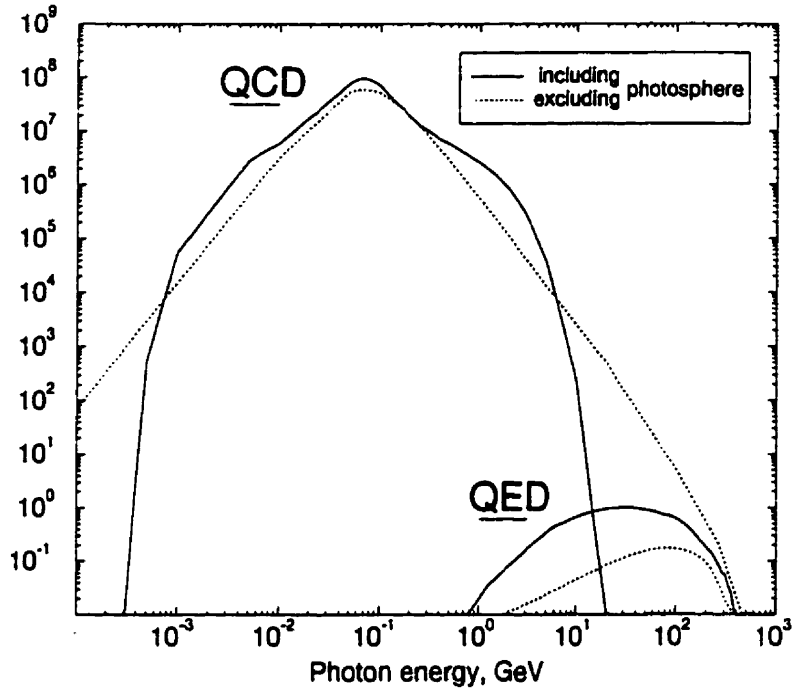

Figure 6.5: Photon emission spectrum from $T = 50$ GeV ($M = 2 \times 10^{12}$g). Solid lines are spectra which include photospheres (QCD or QED). Dotted lines are given for comparison and represent the results for photons from direct quark fragmentation at the horizon and subsequent π^0 decay (QCD), and for direct photon emission neglecting the QED photosphere (QED).

We notice that the photon spectrum from the QCD photosphere peaks at about 100 GeV. The same occurs also for other black hole temperatures due to the fact that these photons are produced by the isotropic decays of neutral pions. In fact, $E_{peak} = 70$ MeV $\simeq m_{\pi_0}/2$. The number of these QCD-induced photons is several orders of magnitude greater than the number produced at the horizon or in the QED photosphere.

An obvious difference between the decay photon spectra with and without the QCD photosphere is the slope of the distribution at both high and low energies. It is much steeper when the photosphere formation is taken into account. Subsequently, significantly more higher energy photons were predicted from a black hole of a given

temperature without photosphere. More important still, our results for different fixed black hole temperatures show that as the black hole becomes hotter, the spectrum at the extremes flattens if the photosphere effect is ignored, whereas the slope stays the same otherwise. This is due to the fact, that this slope is inverse proportional to the peak energy of the quark gluon distribution before hadronization. The peak energy of the Hawking distribution is proportional to the black hole temperature, whereas the peak energy of the distribution at the photosphere edge is constant.

An interesting question for further study is how the photon spectrum varies with T_{BH} for a wide range of black hole temperatures. This would make it possible to predict the lifetime-integrated photon spectrum of a black hole with specified initial mass. That information, together with assumptions about the mass distribution of primordial black holes, would allow us to estimate their contribution to the diffuse intergalactic γ-ray background. Heckler finds that this contribution is not changed significantly by the photosphere formation effect, but a more detailed check of his estimate would be worthwhile. This work is still in progress.

It should also be noted, that although the QED and QCD photospheres were discussed separately in this thesis, for black hole temperatures $T_{BH} \gtrsim 100$ GeV, the photons emitted from the edge of the QCD photosphere may take part in the interactions inside the QED photosphere. This possibility is also a subject of further study.

Conclusion

Our main results can be summarized as follows. The test-particle method of solving the Boltzmann equation, previously used for analyzing heavy ion collisions, was applied to the problem of black hole evaporation. The method was adopted for the case of steady state diffusion of particles emitted by a microscopic black hole. A code to simulate the bremsstrahlung and pair production interactions of the test particles was developed, leading to solutions for the particle distribution functions at any distance from the black hole horizon.

Simulation of microscopic black hole emission in both QED and QCD energy ranges corroborates the hypothesis of photosphere formation suggested by Heckler in [15]. We find that any black hole of mass $M \leq 5 \times 10^{14}$ g develops a dense cloud of interacting quarks and gluons which extends certain distance from the black hole horizon. The evolution of such small ($r < 0.08$ fm) black holes is dominated by mass loss through Hawking radiation. Part of this radiation is in free quarks and gluons which are processed in the QCD photosphere until their average energy drops to the point $\overline{E} \sim \Lambda_{QCD}$, where they hadronize into stable particles and fast-decaying pions. Another part consists of electrons, positrons and photons. Once the black hole mass drops below $M \sim 2 \times 10^{12}$, these particles interact significantly enough to form another, less dense cloud at a distance about 700 times the horizon radius. This QED photosphere extends over a distance of about 400 fm, where it dissipates and emits much less energetic, but in much larger quantity than originally, electrons, positrons and photons.

Energy distributions of the particles leaving both photospheres were obtained and shown to greatly differ from the original nearly-thermal Hawking distributions by being softened to the much lower average energies of $\sim$ 300 MeV (QCD) and from 100 GeV for a 10^{12} g black hole to the estimated 0.5 MeV for a 10^{6} g black hole (QED). Finally, an estimate for the photon spectrum emitted from both QED and QCD photospheres of an individual fixed temperature black hole was made, which provides the basis for a calculation of the lifetime-integrated spectrum of a black hole. It is possible that such a calculation will somewhat soften previous constraints on the total density of primordial black holes in the universe.

Bibliography

[1] Hawking, S.W. Commun. Math. Phys. **43**, 199 (1975).

[2] Halzen, F., Zas, E., MacGibbon, J.H. and Weekes, T.C. Nature (London) **353**, 807 (1991).

[3] Carr, B.J. in *Observational and Theoretical Aspects of Astrophysics and Cosmology* (eds. Sanz J.L. and Goicoechea L.J.) 1 (World Scientific, Singapore, 1985).

[4] Hawking, S.W. Mon. Not. R. astr. Soc. **152**, 75 (1971).

[5] Bullock, J.S. and Primack, J.R. Phys. Rev. D **55**, 7423 (1997).

[6] Schutz, B.F. *A first course in general relativity* (Cambridge University Press, 1990).

[7] Hawking, S.W. Nature **248**, 30 (1974).

[8] Carr, B.J. Astr. J. **206**, 8 (1976).

[9] Page, D.N. and Hawking, S.W. Astr. J. **206**, 1 (1976).

[10] Page, D.N. Phys. Rev. D **13**, 198 (1976).

[11] Turner, M.S. Nature **297**, 379 (1982).

[12] MacGibbon, J.H. and Weber, B.R. Phys. Rev. D **41**, 3052 (1990).

[13] MacGibbon, J.H. and Carr, B.J. Astrophys. J. **371**, 447 (1991).

[14] Oliensis, J. and Hill, C.T. Phys. Lett. B **143**, 447 (1984).

[15] Heckler, A.F. Phys. Rev. D **55**, 480 (1997).

[16] Walke, G.M. McGill University Ph.D. Thesis (1990).

[17] Jauch, J.M. and Rohrlich, F. *The Theory of Electrons and Photons* (Springer-Verlag, New York, 1975).

[18] Haug, E. Z. Naturforsch. Teil A **30A**, 1099 (1975).

[19] Weldon, H.A. Phys. Rev. D **26**, 2789 (1982).

[20] Joseph, J. and Rohrlich, F. Rev. Mod. Phys. **30**, 354 (1958).

[21] Bertsch, G.F. and Das Gupta, S. Phys. Reports, **160**, 191 (1988).

[22] Goldstein, H. *Classical Mechanics, Second Edition* (Addison-Wesley, 1980).

[23] Halzen, F. and Martin, A.D. *Quarks and Leptons* (John Wiley and Sons, 1984).

[24] Heckler, A.F. Phys. Rev. Lett. **78**, 3430 (1997).